



Michigan Technological University
Create the Future Digital Commons @ Michigan Tech

Dissertations, Master's Theses and Master's
Reports - Open

Dissertations, Master's Theses and Master's
Reports

2013

Determining the Effect of Thermal Treatment Timing on Ultra-High Performance Concrete Beams

Christopher H. Mullen
Michigan Technological University

Follow this and additional works at: <https://digitalcommons.mtu.edu/etds>



Part of the [Civil Engineering Commons](#)

Copyright 2013 Christopher H. Mullen

Recommended Citation

Mullen, Christopher H., "Determining the Effect of Thermal Treatment Timing on Ultra-High Performance Concrete Beams", Master's Thesis, Michigan Technological University, 2013.
<https://doi.org/10.37099/mtu.dc.etds/741>

Follow this and additional works at: <https://digitalcommons.mtu.edu/etds>



Part of the [Civil Engineering Commons](#)

DETERMINING THE EFFECT OF THERMAL TREATMENT TIMING ON
DEFLECTIONS OF ULTRA-HIGH PERFORMANCE CONCRETE BEAMS

By

Christopher H. Mullen

A THESIS

Submitted in partial fulfillment of the requirements for the degree of

MASTER OF SCIENCE

In Civil Engineering

MICHIGAN TECHNOLOGICAL UNIVERSITY

2013

© 2013 Christopher H. Mullen

This thesis has been approved in partial fulfillment of the requirements for the Degree of
MASTER OF SCIENCE in Civil Engineering

Department of Civil and Environmental Engineering

Thesis Advisor: *Dr. Tess Ahlborn*

Committee Member: *Dr. Lawrence Sutter*

Committee Member: *Dr. Michele Miller*

Department Chair: *Dr. David W. Hand*

Table of Contents

Table of Contents.....	iii
List of Figures	v
List of Tables	vi
Acknowledgements	vii
Abstract.....	viii
Chapter 1 Introduction and Motivation	1
1.1 Background.....	1
1.2 Need for Research.....	4
1.3 Thesis Objective and Scope	5
1.4 Thesis Outline	6
Chapter 2 Literature Review	7
2.1 Fundamentals of Concrete Compressive Creep	7
2.1.1 Material Influences	8
2.1.2 Environmental Factors.....	10
2.2 Creep Testing Methods.....	10
2.3 Ultra High-Performance Concrete (UHPC).....	12
2.3.1 UHPC History	12
2.3.2 UHPC Composition	15
2.3.3 UHPC Material Properties.....	16
2.4 UHPC Creep Research	18
2.5 Prestress Loss and Deflection Analysis.....	25
2.5.1 Normal Strength Concrete Models for Determining Prestress Losses.....	26
2.5.2 Normal Strength Concrete Models for Determining Deflections	31
2.6 Deflection Data from UHPC bridges	34
2.7 Current UHPC Design codes	38

Chapter 3 Analytical Plan.....	41
3.1 Modeling UHPC Time Dependent Properties.....	41
3.1.1 UHPC Creep Model	41
3.1.2 UHPC Shrinkage Modeling	42
3.1.3 Modeling Elastic Modulus	42
3.2 Selection of Beam Shapes for Analysis	43
3.3 Prestress Loss Calculation Methods	47
3.3.1 Modeling for Ambient Curing Conditions of UHPC.....	50
3.3.2 Modeling for Thermal Treatment Curing Conditions	51
3.4 Short and Long-term Deflection.....	54
Chapter 4 Results and Discussion	56
4.1 Bulb Tee Section Results	57
4.2 Pi-girder Results	59
4.3 Discussion of Results	62
4.3.1 Strand Stress.....	63
4.3.2 Prestress Losses	65
4.3.3 Short and Long-Term Deflections	67
Chapter 5 Conclusions and Future Work.....	69
5.1 Conclusions	69
5.2 Future Work.....	70
References	71
Appendix A - Prestress Losses Matlab Program	77
Appendix B – Results of Rectangular Beam	82
Appendix C – Copyright Permissions.....	85
Appendix D – Sample Calculation for Rectangular Beam.....	86

List of Figures

Figure 1.1 Prestressed Concrete Concept.....	2
Figure 2.1 Creep frames used by Flietstra (2011)	20
Figure 2.2 Modified Bulb Tee for Wapello Co. Bridge Girders (Wipf et al. 2009)	36
Figure 2.3 2nd Generation Pi-Girder (Rouse et al. 2011)	37
Figure 3.1 Cross Section of Modified Iowa Bulb Tee Girder (Wipf et al. 2009).....	45
Figure 3.2 Cross Section of Pi-Girder.....	46
Figure 3.3 Cross Section of Composite Shape of Bulb Tee Section	46
Figure 3.4 Creep Strain Models for Ambient Cured UHPC.....	52
Figure 3.5 UHPC Shrinkage Strain Models used in Prestress Losses Analysis.....	53
Figure 3.7 Modulus of Elasticity Models used in Prestress Losses Analysis	54
Figure 4.1 Prestress Loss and Deflection Results for Bulb Tee Section - Ambient Cure.....	57
Figure 4.2 Strand Stress and Deflection for Modified Bulb Tee Thermally Treated at 48 Hours	58
Figure 4.3 Strand Stress and Deflection for Modified Bulb Tee Thermally Treated at 30 Days	59
Figure 4.4 Strand Stress and Deflection for Pi-girder Beam with Ambient Cure	60
Figure 4.5 Strand Stress and Deflection for Pi-girder Beam Thermally Treated at 48 Hours	61
Figure 4.6 Strand Stress and Deflection for Pi-girder Beam Thermally Treated at 30 Days..	62
Figure B.1 Prestress Losses and Deflections for Ambient Cured Rectangular Section.....	82
Figure B.2 Strand Stress and Deflections for Rectangular Beam Thermally Treated at 48 Hours	82
Figure B.3 Strand Stress and Deflections for Rectangular Beam Thermally Treated at 30 Days.....	83

List of Tables

Table 2.1 List of UHPC Bridge Projects in United States as of 2012	14
Table 2.2 Typical Ductal Composition, BSI 1000	16
Table 2.3 Typical UHPC Mechanical Properties	17
Table 3.1 Shape Properties used for Prestress Loss Analysis	44
Table 4.1 Strand Stress at Critical Time Steps	64
Table 4.2 Prestress Losses as Percentage of Initial Strand Stress	66
Table 4.3 Deflections at Critical Time Steps	68
Table B.1 Select Results for Strand Stress and Deflections of Ambient Cured Rectangular Section.....	84
Table B.2 Select Results for Strand Stress and Deflections of Ambient Cured Rectangular Section... ..	84
Table B.3 Select Results for Strand Stress and Deflections of Ambient Cured Rectangular Section.....	84

Acknowledgements

The author would like to thank his advisor, Dr. Tess M. Ahlborn at Michigan Technological University for her guidance throughout this research. He would also like to thank his other committee members, Dr. Lawrence Sutter and Dr. Michele Miller, for their assistance. He would also like to thank the Civil and Environmental Engineering Department at Michigan Tech for the partial financial support during his MSCE program.

The author would also like to give a special thank you to his fiancé, Rachele, for all of her love and support as well as his family and friends.

Abstract

The loss of prestressing force over time influences the long-term deflection of the prestressed concrete element. Prestress losses are inherently complex due to the interaction of concrete creep, concrete shrinkage, and steel relaxation. Implementing advanced materials such as ultra-high performance concrete (UHPC) further complicates the estimation of prestress losses because of the changes in material models dependent on curing regime.

Past research shows compressive creep is “locked in” when UHPC cylinders are subjected to thermal treatment before being loaded in compression. However, the current precasting manufacturing process would typically load the element (through prestressing strand release from the prestressing bed) before the element would be taken to the curing facility.

Members of many ages are stored until curing could be applied to all of them at once. This research was conducted to determine the impact of variable curing times for UHPC on the prestress losses, and hence deflections.

Three UHPC beams, a rectangular section, a modified bulb tee section, and a pi-girder, were assessed for losses and deflections using an incremental time step approach and material models specific to UHPC based on compressive creep and shrinkage testing. Results show that although it is important for prestressed UHPC beams to be thermally treated, to “lock in” material properties, the timing of thermal treatment leads to negligible differences in long-term deflections. Results also show that for UHPC elements that are thermally treated, changes in deflection are caused only by external loads because prestress losses are “locked-in” following thermal treatment.

Chapter 1 Introduction and Motivation

1.1 Background

Prestressed concrete was the most significant change in building materials at the beginning of the 20th century, allowing engineers and architects to test the structural limits of concrete construction. Longer spans and more efficient shapes pushed the realm of possibility for designers. The first engineer to present the idea of prestressing concrete was P.H. Jackson in 1888 (Dinges 2009). Unfortunately, the lack of high strength steel prevented the idea from becoming much more than that.

Eugene Freyssinet further pursued the idea of prestressed concrete and patented the idea in 1928. During the following years, Freyssinet stated the need for high strength materials to overcome the loss of tension in the prestressing steel. He was the first engineer to recognize that concrete creep influenced prestress losses. Although Freyssinet patented the idea, prestressed concrete was brought to a halt by the lack of funding and advanced materials needed to promote the concept (Dinges 2009).

Gustave Magnel, a research professor in Germany during World War II, was able to perform full scale testing on prestressed beams and further develop the concept with relation to material properties. He proved that prestressed losses had a very important impact on prestressed concrete design. At the end of the war, Magnel successfully began using prestressed concrete in bridges and other infrastructure that was used to rebuild Europe. In

1951, with Magnel as the chief designer, the Walnut Lane Bridge was the first prestressed concrete bridge completed in the United States. (Dinges 2009)

Figure 1.1 depicts the concept of prestressing. Part A of the figure shows the concrete element in the prestressing bed where the section is cured until the concrete can withstand the required stresses brought on by release of prestressing strands. Part B depicts the beam when the pretensioned strands are released from the bed. The upward deflection, or camber, is caused by the compressive force that is eccentric to the center of gravity of the concrete. Part C of Figure 1.1 shows the beam in service. Due to the prestressing the beam will exhibit compressive stress in the bottom fibers of the beam. This method is inherently ideal for concrete as its potential to carry compressive stress is its best attribute.

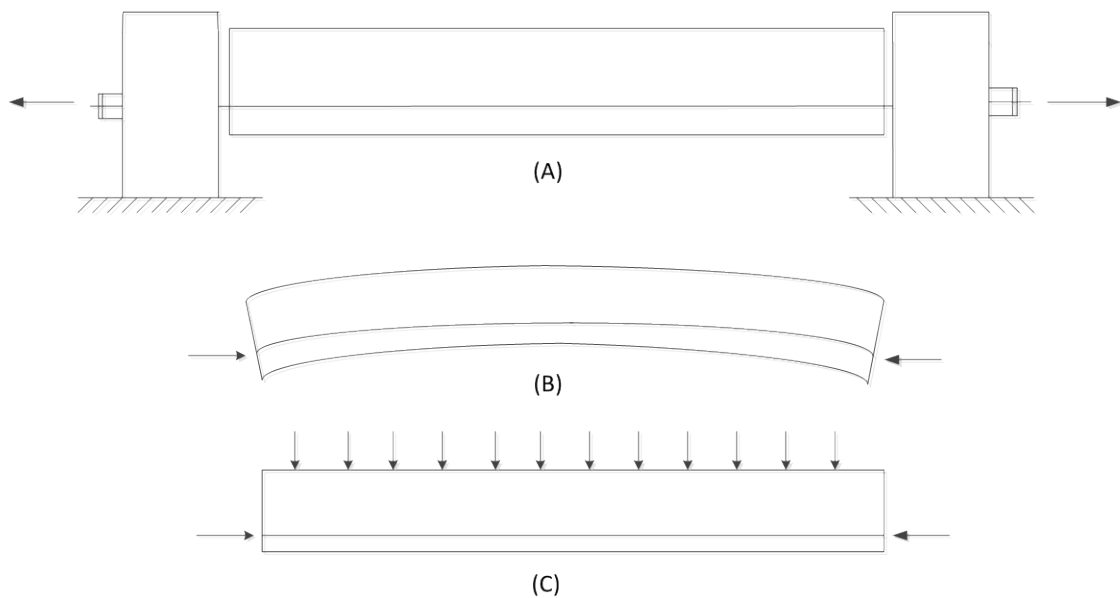


Figure 1.1 Prestressed Concrete Concept

As seen from the history of prestressed concrete, stronger materials lend themselves well to the prestressing procedure. Current prestressing procedures employ the use of concrete with high compressive strengths (up to 12,000 psi) and steel with high tensile capacities (Grade

270 and 300) with ultimate strength of 270,000 psi and 300,000 psi, respectively. With the use of additives, concrete plants starting to achieve 1-day compressive strengths up to 8,000 psi.

Ultra high performance concrete (UHPC) was developed in Europe in the 1990's where it was first known as reactive powder concrete (RPC). Since its introduction, UHPC has been a material which has sparked interest in research throughout the world. ACI Committee 239 has published this definition of UHPC as concrete that has a minimum specified compression strength of 22,000 psi with specified durability, tensile ductility and toughness requirements; fibers are generally included to achieve specified requirements. The high strength of this material is achieved through dense particle packing which implies high durability, improved freeze-thaw resistance, increased resistance to various chemicals, and higher penetration resistance (Wille et al. 2011). The improved tensile properties are achieved through steel fiber reinforcement. The properties of UHPC make it appealing to the prestressed concrete industry because it allows for higher prestressing forces and decreased amounts of concrete. The long-term durability also provides potential for bridges with a 100 year service life or longer (Ahlborn et al. 2008).

Due to a very low w/c ratio in UHPC, as low as 0.14, the cement does not reach full hydration. However, it has been observed that by applying a thermal treatment UHPC exhibits improved performance. (Loukili et al. 1998; Kollmorgen 2004; Graybeal 2006).. Thermal treatment allows for continued hydration of the cement particles and increased pozzolanic reaction of the silica fume (Cheyrezy et al. 1995). The thermal

treatment is also beneficial for increasing the rate at which these reactions take place. The recommended thermal treatment is $195^{\circ} \pm 3^{\circ}$ at $95 \% \pm 3\%$ relative humidity.

1.2 Need for Research

Advancement in concrete materials has led to the ability to develop products that significantly out-perform traditional concrete in nearly every measurable standard. Although this development is positive for the construction industry, it is important for these new materials to be well understood because of their impact on safety and expense. The use of UHPC is specifically of interest to the prestressing industry and the industry continues to gain confidence as the behavior of UHPC is better understood.

Prestress losses are of particular interest with this new material because deflections are affected by losses, which in turn are affected by mix design, curing, and concrete strength among others. Previous research has concluded that creep and shrinkage exhibited by UHPC would be “locked-in” if the concrete was subjected to thermal treatment in the precasting procedure (Flietstra 2011). This appears to be true for specimens that are thermally treated before being loaded in compression but this is not consistent with current prestressing facilities. Precast facilities in the U.S. build the element first, including loading the element in compression at the time of prestressing release, prior to thermal treatment. UHPC research at Michigan Tech has shown that creep and shrinkage are important to consider when UHPC is tested mimicking prestressing industry practices (Flietstra 2011). However, no previous research has addressed the impact of timing of thermal treatment on the prestress losses and consequently, the estimated short and long-term deflections.

1.3 Thesis Objective and Scope

The objective of this research is to determine the impact that timing of thermal treatments can have on short-term and long-term deflections of three UHPC beams. This research aims to model the creep, shrinkage, and modulus of elasticity data collected by previous research at Michigan Tech and incorporate the models for predicting deflections.

This document reviews literature on the fundamentals of compressive creep of concrete, current ASTM creep testing standards, UHPC material properties, the current state of UHPC compressive creep research, and various methods for analyzing prestress losses. The literature review also discusses current UHPC design codes and how prestress losses are being considered in those codes.

Prestress losses are estimated for three UHPC beams. The analysis uses compressive creep data sets from UHPC cylinders obtained during and after curing regimes that replicate industry practice. The curing regimes are those that were tested by Flietstra (2011). The data is used to fit compressive creep function curves for ambient cured and thermally treated conditions. The three scenarios investigated are a rectangular solid beam, a bulb tee girder, and a 2nd generation Pi-girder designed by FHWA specifically for UHPC (Graybeal 2009b). The first generation of this shape is documented by the FHWA as well (Graybeal 2009a). This analysis of the prestressed losses utilizes an incremental time-step approach to calculate short and long-term losses taking into account the different properties of UHPC at both early age and long-term. Deflections are then calculated from traditional methods.

Deflections are directly impacted by prestress losses. This research will show whether the timing of thermal treatment, or in other words the manufacturing process, has a measureable influence on short-term and long-term deflections.

1.4 Thesis Outline

Chapter 2 of this thesis is a literature review of publications relevant to the material discussed in the remainder of the document, including creep and shrinkage models, and UHPC background. Chapter 3 discusses the analytical methods used to determine losses and deflection for three UHPC beams. Chapters 4 and 5 present and discuss the results of losses and deflections from the different curing regimes tested. The final chapter (6) offers recommendations for future work related to this paper. Appendices with sample calculations are included for completeness.

Chapter 2 Literature Review

2.1 Fundamentals of Concrete Compressive Creep

When concrete is stressed it exhibits an instantaneous strain. When that stress is sustained over a period of time, the concrete undergoes additional strain which is referred to as creep. Creep can be considered in several phases through the loading history of the specimen. After the instantaneous strain or initial creep, the specimen will deform over time due to basic creep and shrinkage. The creep coefficient at any time is the basic creep strain at that time divided by the initial strain of the specimen. Creep may be observed at all stress levels and under any type of loading scenario (compression, bending, tension, etc.). The amount of creep strain the concrete will exhibit is dependent on several characteristics including magnitude of sustained load, duration of load, age of loading, and several of the concrete properties (Nawy 2010). Although it is preferred to consider the properties one at a time, most concrete properties are covariant and changing one variable can have a significant effect on other variables (Neville 1970).

Several factors can have an influence on concrete creep, but can essentially be divided into two distinct categories. The first category includes all material influences that stem from constituents in the concrete mix, their proportions, and the applied stress. The latter category includes environmental factors such as moisture exchange and temperature.

2.1.1 Material Influences

The properties of the normal strength concrete matrix are very influential in determining the creep potential of concrete. The content of the cement paste in the concrete plays a large role in determining creep properties because when loaded at stress levels comparable to the cement paste, the aggregate does not creep. The driving force behind the cement paste creep is that after a sustained stress, the physically absorbed water is forced out of the C-S-H compound causing a creep strain (Mehta and Monteiro 2006). Although moisture movement plays a large role in concrete creep, it is not the only contributing factor. The interfacial transition zone (ITZ) is the area around the large aggregate that is hydrated differently than the bulk cement paste and is, therefore, less dense. This zone is commonly the weakest point in the concrete microstructure. At higher stress levels, greater than 30 or 40 percent of ultimate stress, the microcracks in the ITZ have experimentally shown significant creep (Mehta and Monteiro 2006). It was also proven that rapidly hardening cements provide less potential for creep (Neville 1970). Neville's tests were performed at similar ages and with similar applied stress, showing that the more hardened cement paste exhibited less creep. These tests also showed that portland-pozzolan mixtures were more likely to creep than portland cement mixtures.

In regards to normal strength concrete, several authors have concluded that the unhydrated cement content will act in a manner similar to aggregate. Neville suggested that creep of concrete and cement paste can be related to the sum of aggregate and unhydrated cement contents (Neville 1970), and Powers concluded with regards to shrinkage that any

unhydrated cement be considered a part of the aggregate (Mehta and Monteiro 2006). While very little research has been done to define creep in UHPC, these concepts are important when describing the creep of UHPC because of the large amount of unhydrated cement in the concrete matrix.

The stress-strength relationship plays an important role in the creep behavior of the specimen. Although it is well understood and proven that creep is proportionally related to applied stress and inversely related to strength, the range in which this relationship is linear is not fully understood. Linearity has been observed to have an upper limit with stress-strength ratios from 0.3 to 0.75 (Neville 1970). As Neville also notes, micro cracking generally takes place in a concrete compression specimen at stress-strength ratios of 0.4 to 0.6. It is not surprising that once microcracks begin to develop that creep would increase more rapidly. This behavior becomes more relevant to UHPC because UHPC is a very homogeneous material compared to normal strength concrete, and therefore, will be less likely to form microcracks. UHPC is typically fiber reinforced and the fibers bridge the gaps between microcracks upon formation to carry the tensile stresses across these cracks.

The relationship between the age of loading and the creep potential is also interesting to point out. For the same stress-strength ratios at time of loading, specimen that were loaded earlier showed less creep than specimen loaded later in their strength gain (Neville 1970). The reason for this is the specimen continues to gain strength and several days after the specimen was loaded, the stress-strength ratio is inherently lower.

2.1.2 Environmental Factors

Environmental factors, such as relative humidity and temperature of storage, play an important role in the creep of concrete. The relative humidity in which the concrete is stored can have a significant impact on the amount of creep. Troxell showed that at a relative humidity of 50%, creep may be two to three times greater than at a relative humidity of 100% (Neville 1970). Sometimes, like in the case of precast elements, the storage humidity can be controlled, but with cast-in-place applications humidity may be more variable during curing. Although less of an influence on creep, temperature has also been shown to have an effect. Through experimentation, compressive creep of normal strength concrete has been shown to be proportional to the surrounding temperature at which the load is applied (Neville 1970). The relationships between environmental factors and normal strength concrete compressive creep are important to consider because thermal treatments use high temperatures in combination with high humidity to increase the rate of hydration or to “lock in” time dependent properties of UHPC.

2.2 Creep Testing Methods

Standards are available for testing compressive creep for normal strength concrete, and while no such standards exist for UHPC, some can be modified to help characterize UHPC in compressive creep.

The American Society for Testing and Materials (ASTM) is the organization that publishes the most commonly used set of testing standards in the United States. The organization

strives to improve product quality, enhance safety, facilitate market access and trade, and build consumer confidence in products. When industries attempt to achieve widespread consumption of new technology or new products it is beneficial to come together with ASTM to achieve standardization goals.

ASTM C512/C512M-10 is the Standard Method for Creep of Concrete in Compression (ASTM 2013). The purpose of this test is to determine the compressive creep strain in normal strength concrete. The results of this test can be used to compare the creep potentials of different concretes. ASTM C512 describes loading procedures, specimen sizes, and testing apparatus's with regards to the testing of normal strength concrete. With few modifications, ASTM C512 has been used in UHPC creep research with much success (Flietstra 2011). Modifications that are important to consider when testing UHPC are the applied level of load, creep frame rigidity, preliminary static compressive testing, and the casting of specimens for testing. ASTM C512 calls for a compressive creep load no greater than 40 percent of current compressive strength. To provide information relevant to the prestressing facility the stress induced by the creep frame was increased to 60 percent of current compressive strength of the cylinder, which is the maximum concrete stress allowed at time of release of prestressing strands as prescribed by ACI (ACI 318-11). A combination of high concrete stress level and increased stress capacity of UHPC calls for larger loads to be placed on the UHPC cylinders, as compared to normal strength concrete specimens. For this reason it is important the creep frames used for UHPC compressive creep testing are able to maintain high compressive loads at a constant level while remaining rigid. Previous

UHPC research resulted in the design of creep frames and hydraulic pumps to maintain this constant load (Nyland 2008, Flietstra 2011).

Before loading the specimen for compressive creep testing, it is necessary to know the current compressive strength of the specimen. ASTM C39 is the accepted standard for testing the compressive strength of normal strength concrete cylinders. Similar to compressive creep testing, modifications were made to ASTM C39 to account for the differences in normal strength concrete and UHPC. Modifications include increasing the load rate from 35 psi/s to 150 psi/s and using 3 x 6 in cylinders instead of 4 x 8 in or 6 x 12 in cylinders (Kollmorgen 2004). It should also be noted that previous UHPC research has used horizontally casted steel molds (Flietstra 2011). The reasoning for horizontal molds was to ensure planeness on either end of the section without the need for end grinding, especially with time of loading being a critical factor and end grinding being time consuming.

No ASTM standards exist with regards to mixing and curing UHPC materials or test specimens, but suggested methods are available for both mixing and curing through individual manufactures.

2.3 Ultra High-Performance Concrete (UHPC)

2.3.1 UHPC History

After being introduced by the French in 1990, ultra high performance concrete has been slow to hit the market in the United States. With a lack of design codes in the United States, designers and researchers are using design codes that are being developed across the world

to introduce UHPC to the United States infrastructure. To date, nearly 20 bridges in the United States have incorporated UHPC in construction using two primary techniques. The first is complete UHPC construction in which the bridge uses UHPC for either the bridge girders or both the bridge girders and bridge deck. The second application of UHPC has been the use of thin overlays or full depth joints between girders.

Two bridges in Iowa and one bridge Virginia have used UHPC bridge girders. The Wapello County Bridge in Iowa and the Cat Point Creek Bridge in Virginia were the first two uses of UHPC bridge girders in the United States and both utilized 45 inch deep bulb tees (Graybeal 2013). The third bridge to use UHPC girders, also in Iowa, was the Jakway Park Bridge. This application used an innovative pi-girder in an attempt to optimize the material performance of UHPC (Graybeal 2013).

Numerous other applications have used ultra-high performance concrete in the U.S. Most of this work has been done by the New York DOT and the Iowa DOT. Applications include waffle deck panels, full depth joints between deck panels, full depth joints between girders, and shear connections to girders. Table 2.1 lists construction involving UHPC as well as references for each project (Graybeal 2013).

Table 2.1 List of UHPC Bridge Projects in United States as of 2012

Name	Year	Application	Reference
Mars Hill Bridge, Wapello County , IA	2006	Three 45-in-deep bulb-tee beams	Bierwagon (2005)
Route 624 over Cat Point Creek, Richmond County, VA	2008	Five 45-in-deep bulb-tee beams	Ozyildirim (2011)
Jakway Park Bridge, Buchanan County, IA	2008	Three 33-in-deep pi shaped girders	Keierleber (2010)
State Route 31 over Canadaigua Outlet, Lyons, NY	2009	Joints between deck bulb tees	Shutt (2009)
State Route 23 over Otego Creek, Oneonta, NY	2009	Joints between full-depth deck panels	Royce (2011)
Little Cedar Creek, Wapello County, IA	2011	Fourteen 8-in-deep waffle deck panels	Moore (2012)
Finderboard Road Bridge over Staten Island Expressway, NY	2011 to 2012	Joints between deck bulb tees	Royce (2011)
State Route 248 over Bennett Creek, NY	2011	Joints between deck bulb tees	Royce (2011)
U.S. Route 30 over Burnt River and UPRR bridge, Oregon	2011	Haunch and shear connectors and transverse joints	Bornstedt (2011)
U.S. Route 6 over Keg Creek, Pottawatomie County, IA	2011	Longitudnal and transverse joints between beams	Anon
Ramapo River Bridge, Sloatsburg, NY	2011	Joints between full-depth deck panels	Anon
State Route 42 Bridges (2) near Lexington, NY	2012	Joints between full-depth deck panels and shear pockets	Anon
State Route 31 over Putnam Brook near Weedsport, NY	2012	Joints between full-depth deck panels	Anon
I-690 Bridges (2) over Peat Street near Syracuse, NY	2012	Joints between full-depth deck panels	Anon
I-690 Bridges (2) over Crouse Avenue near Syracuse, NY	2012	Joints between full-depth deck panels	Anon
I-690 Bridge over Kirkville Road near Syracuse, NY	2012	Joints between full-depth deck panels	Anon

Windham Bridge over BNSF Railroad on U.S. Route 87 near Moccasin, Montana	2012	Joints between full-depth deck panels and shear connections to beams	Anon
---	------	--	------

Although several commercially available UHPC premix blends are available worldwide, the only available UHPC in the U.S. at the time of creep testing by Flietstra was Ductal[®], a product of Lafarge (Flietstra 2011). The research presented herein develops models using data collected from Ductal[®] specimens.

2.3.2 UHPC Composition

UHPC is able to obtain the impressive mechanical properties by taking advantage of a low water to cement ratio and a very dense microstructure. This is achieved by eliminating the coarse aggregates and using very small particles. The matrix has very few voids and the void system is discontinuous. Additionally, fiber reinforcement is added to the mixture which improves tensile strength by bridging the cracks in the concrete. The composition of Ductal[®] is presented in Table 2.2, showing many of the same constituents that are used in normal strength concrete but with different proportions. The materials selected in UHPC are chosen based on particle size and shape to optimize the particle packing in the concrete. The dry ingredients of the product are shipped in a bag, and are pre-mixed. The fibers and superplasticizer are delivered separately. Water, superplasticizer, and steel fibers are added to the mixture during the mixing procedure.

Table 2.2 Typical Ductal Composition, BSI 1000

Constituent	Proportion (lb/yd³)	Percent by Weight
Sand	1719	41.1
Cement	1197	28.6
Silica Fume	388	9.3
Ground Quartz	354	8.5
Metallic Fibers (8x10 ⁻³ -in dia by 0.5-in long)	270	6.4
Water	236	5.6
Superplasticizer	22	0.5

2.3.3 UHPC Material Properties

Extensive research has been conducted to test the mechanical properties of UHPC for structural design. The Federal Highway Administration (FHWA) has tested UHPC specimens for compressive strength, tensile strength, modulus of elasticity, Poisson's ratio, fatigue behavior, thermal properties, bond strength, impact resistance, early-age creep, and shrinkage (Graybeal 2013). The results of this testing was published as ranges for each of the mechanical properties. Table 2.3 summarizes the results obtained by FHWA (Graybeal 2013).

Table 2.3 Typical UHPC Mechanical Properties

Property	Range
Compressive Strength	20 to 30 ksi
Tensile cracking strength	0.9 to 1.5 ksi
Modulus of elasticity	6,000 to 10,000 ksi
Poisson's Ratio	0.2
Coefficient of thermal expansion	$5.5 \text{ to } 8.5 \times 10^{-6}/^{\circ}\text{F}$
Creep Coefficient	.2 to .8
Specific creep	$4 \times 10^{-8} \text{ to } 3 \times 10^{-7}/\text{psi}$
Total shrinkage	Up to .0009

Others have published results showing the mechanical properties they obtained throughout extensive testing of Ductal[®]. These results are similar to the ranges obtained by Graybeal.

The most important mechanical properties with regards to this research are the elastic modulus increase with time and the early age compressive strength gain. The elastic modulus has an effect on the amount of creep a specimen will endure and rapid strength gain gives the prestressing plant the ability to load elements sooner (by releasing strands at transfer) and increasing production without increasing plant size. Although this may be beneficial to the plant, precautions have to be considered when loading prestressed elements so early in their strength gain. A time dependent study of elastic modulus is important if trying to measure prestress losses when the specimen is loaded at a very early age. Peuse completed extensive compressive strength and modulus of elasticity testing on UHPC in 2006 at Michigan Tech (Peuse 2008, Ahlborn et al. 2011). Peuse examined mechanical properties at ages 3, 7, 14, and 28 days using four curing regimes. The curing regimes were

an ambient cure, a thermal treatment, a delayed thermal treatment, and a double delayed thermal treatment. The delayed thermal treatment and double delayed thermal treatments were started at 10 days and 24 days, respectively, after mixing. The results of this work showed results similar to the results obtained by Graybeal and Lafarge as shown in Table 2.3.

2.4 UHPC Creep Research

Compressive creep models of ultra-high performance concrete are very limited compared to normal strength concrete models. Each case uses specific mix proportions, curing conditions, and testing procedures that impacted the results. These factors along with the results and associated creep coefficients are discussed below. The creep coefficient is commonly used to reference the creep potential of the material and is defined as the creep strain of the specimen at 28 days of loading divided by the initial strain induced initially by sustained loads.

Flietstra (2011) was the first to complete UHPC compressive creep research that took into consideration loading the specimens before and during the application of thermal treatment. The loading plan was done to mimic the loading procedure commonly used in the precasting/prestressing plant. The curing regimes also were designed to mimic the prestressing plant procedures. The regimes included ambient cure, pre-steam with a thermal treatment, standard thermal cure, pre-steam with a delayed thermal cure, and pre-steam with a double delayed thermal cure. Pre-steam environment was 100% relative humidity and 140°F, and the thermal treatment was 100% relative humidity and 198°F. The ambient

cured specimens were in an ambient environment (50% R.H. and 70°F) throughout the curing and loading of the concrete. The standard thermal cure specimen had no treatment until the time of creep loading, at which point they were thermally treated immediately after being loaded. The pre-steam technique is used in the prestressing plant to increase the rate of hydration and strength gain, therefore allowing for an earlier release time of the prestressing force.

All specimens in Flietstra's research were loaded in compression when they reached strength of 14,000 psi, as recommended by the UHPC manufacturers. For cylinders that were given a pre-steam treatment, the strength of 14,000 psi was reached in 14 to 18 hours. Ambient cured specimens reached 14,000 psi compressive strength in approximately 70 hours. Flietstra loaded the cylinders in the creep frames at these times. Figure 3 shows an image of the creep frames used by Flietstra (2011). Permission for the use of this figure is shown in Appendix C.

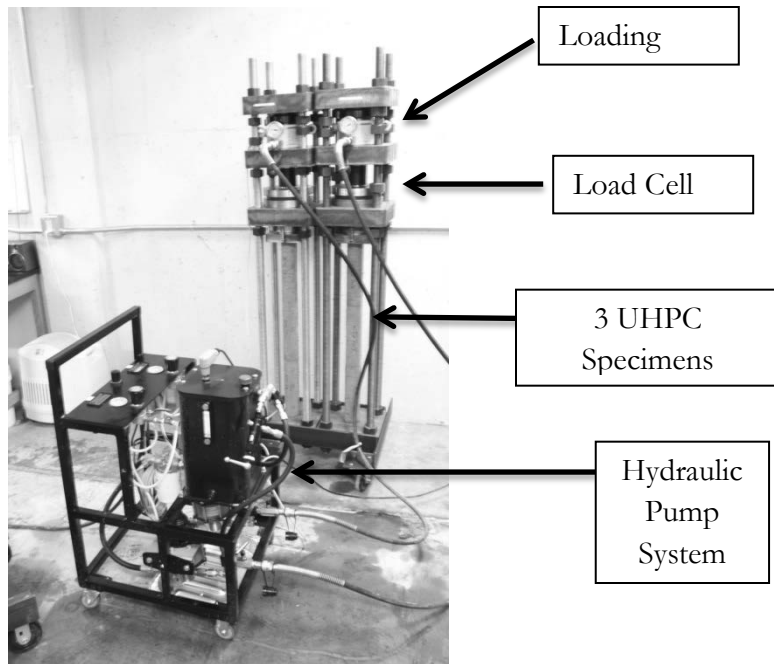


Figure 2.1 Creep frames used by Flietstra (2011)

Flietstra used creep cylinders that were 3 inches in diameter and 12 inches in length. To ensure the ends were parallel, steel horizontal molds were used that were designed to maintain parallel ends without the need to end grind the cylinders. Upon reaching the strength of 14,000 psi, the cylinders were loaded to either 60 percent of the current compressive strength or 20 percent of the current compressive strength. Strains were measured with a Whittemore strain gauge several times during the first week and once a week for a month following. The results of Flietstra's work showed that if UHPC specimens are loaded in compression during or before the thermal treatment is applied, the creep coefficients are much different than what previous researchers have reported for creep coefficients of specimens that were thermally treated before compressive loading. Flietstra found the creep coefficient for thermally treated cylinders to be 1.12 for the $0.6f'_{ci}$ load level (Flietstra 2011).

Graybeal (2006) tested long-term creep and early age high stress creep. The long-term creep testing was conducted according to ASTM C512. The curing regimens used in this testing were ambient cure, steam treated, tempered steam treatment, and delayed steam treatment. For the steam treated and tempered steam treated specimen, the creep loading was initiated 4 days after casting. The delayed steam specimens were loaded 21 days after casting, and the ambient cure specimens were loaded 28 days after being casted. The sizes of the cylinders used in the testing were 4 inches in diameter and 8 inches in height. All of the cylinders were end ground until parallel. The testing results produced final creep coefficients of 0.29 for steam treated specimens, 0.78 for untreated specimen, 0.66 for tempered steam, and 0.31 for delayed steam treatment. From this research it was concluded that if a steam treatment was applied to the specimens before loading, the UHPC exhibited very little creep.

Testing by Graybeal also investigated UHPC that was subjected to compressive loading early in its strength gain (Graybeal 2006). The purpose of this testing program was to answer questions related to the appropriate delay before the transfer of the prestressing force to the prestressed UHPC girder. The two strength levels investigated were 8.6 ksi and 12.5 ksi. The ambient cured specimens were loaded to stress levels ranging from 60 to 90 percent of their current compressive strength and unloaded after 30 minutes of sustained loading. The results showed that specimens loaded at an early age exhibit a large amount of creep strain in the short duration that they are loaded. For comparison, a cylinder that was stressed to a similar stress/strength ratio in the short-term creep testing had a creep coefficient of 0.42, while the long-term steam treated specimen had a creep coefficient of 0.27. These results

emphasized the importance of understanding the early age creep potential and the importance of steam treating specimens that require early age loading (Graybeal 2006).

Another research program that investigated the time dependent deformations of UHPC was started in Germany at the University of Karlsruhe by Burkart and Muller (2008). The purpose of this research was to create a comprehensive database enabling the development of a thermodynamically sound material law for the time- and load-dependent deformation behavior of UHPC. The researchers investigated several parameters which are commonly considered when investigating normal strength concrete creep, including age of loading, storing conditions, specimen size and geometry, and stress level of the concrete. Stress levels were 30 and 60 percent of the compressive strength at the time of loading. The cylinders were loaded at 1, 3, and 28 days. Specimens not loaded at 1 day were moist cured for 2 days then cured in ambient conditions until loaded. Conclusions from this research show that models for normal strength concrete and high strength concrete do not accurately predict the compressive creep behavior of UHPC. Most importantly these results have shown the effects of creep on early age concrete are much more pronounced with UHPC specimens (Burkart and Muller 2008).

The nonlinearity of UHPC creep was also tested by using two stress levels at different loading ages (Burkart and Muller 2008). The reason for this testing was to find a range of service stresses where creep can be assumed to be linearly related to the stress inducing that creep. Because of the high compressive strength of UHPC, it was expected to have a limit above the originally defined range for normal strength concrete or high strength concrete.

The results showed that the relationship between creep deformation and stress was linear up to a stress level of 60 percent of ultimate strength.

Tests were also performed to determine the strength limit under sustained loading (Burkart and Muller 2008). Specimens loaded at an early age (1 day) were shown to carry sustained loads of 90 percent of the current stress capacity (Burkart and Muller 2008). The specimens loaded at 28 days, although there was a large scatter, seem to have a strength limit of approximately 80 percent of the 28 day strength (Burkart and Muller 2008).

Francisco published a research plan in 2009 designed to model the creep and shrinkage of ultra-high performance fiber-reinforced concrete taking into account a moderate heat treatment (Francisco et al. 2012). This moderate heat treatment is used by prestressing facilities to accelerate the hardening of concrete immediately after molding. This treatment is similar to the “pre-steam” treatment that was used by Flietstra (2011).

Francisco constructed two different UHPC mixtures using different types of superplasticizer in each. His work also used two moderate heat treatments. One treatment was a moist environment with a temperature of 50 degrees C and the other was for a shorter duration at a temperature of 65 degrees C. The size of the cylinder used during creep and shrinkage tests were 70 mm in diameter and 220 mm tall. The specimens were loaded to 40% of the compressive strength and were loaded 2 days after molding. A hand ball micrometer was used to measure the strains on 2 or 4 axes. The average 20 hour strength and average 28 day strength of the UHPFRC was 152 MPa (22,000 psi) and 188 MPa (27,000 psi), respectively.

Results obtained for one year showed creep strains of approximately 1000 μm and shrinkage strains of 250 μm (Francisco et al. 2012).

Loukili published his experimental investigation of reactive powder concrete (RPC) in 1998 which aimed to characterize the creep and shrinkage of fiber reinforced RPC after a 90° C heat treatment (Loukili et al. 1998). Two types of cylinders were prepared for this work. For mechanical testing the cylinders measured 110 mm in diameter and 220 mm in height. The cylinders intended for creep and shrinkage testing measured 90 mm in diameter and 600 mm in height. The specimens were cured in water at 20° C for 7 days, placed in 90° C water for 4 days, then air dried at 90° for 2 days. The creep and shrinkage tests were measured with three LVDT sensors separated 120 degrees from each other. The creep specimens were loaded to approximately 20 percent of the compressive strength at the time of loading and remained in the creep frames for 4 months. The mechanical properties of this concrete were similar to the properties in the literature described above with 28 day compressive strength around 160 MPa and Young's modulus around 50 GPa.

The results of the creep testing were compared to similar testing conducted on 3 different high strength concretes and showed the fiber reinforced RPC exhibited significantly higher specific creep in all three cases. Loukili notes this is due to the increased paste content and lack of coarse aggregate in RPC (Loukili et al. 1998).

Garas investigated compressive creep of UHPC using varying curing regimes (Garas et al. 2012). The intent of this work was to incorporate a curing regime that was achievable by most prestressing facilities in the United States. The UHPC supplier recommends a 90

degree C cure which would require most plants to make changes. Compressive creep testing was performed on cylinders measuring 4 inches in diameter by 15 inches tall. The specimens were loaded at 7 days to a load equivalent to 40 percent of the 7-day compressive strength. The strain was measured for 1 year after loading. The measured specific creep ($\mu\epsilon$ divided by applied stress) for the 90° C thermal treatment, the 60° C thermal treatment, and the ambient cure was 22.6 $\mu\text{m}/\text{ksi}$, 28.5 $\mu\text{m}/\text{ksi}$, and 59.8 $\mu\text{m}/\text{ksi}$, respectively. These results show that decreasing the temperature of thermal treatment had a significant effect on the creep results. Garas's work also reinforced the importance that thermal treatment can have on the amount of creep strain that UHPC will undergo (Garas et al. 2012).

Numerous researchers have recognized the issue of integrating current precast plant procedures into laboratory test methods such as defining compressive creep and corresponding drying shrinkage. However, no analysis has been documented that considers the impact of the creep testing results and curing regimes on long-term losses and deflections.

2.5 Prestress Loss and Deflection Analysis

Prestress losses are due to the complex interaction of elastic shortening, concrete creep and shrinkage, and steel relaxation. This section outlines the methods considered and used in the analysis of prestress losses and deflections for 3 UHPC beams. It should be noted that most of the methods outlined in this section were formulated for normal strength concrete and were adapted to more accurately model ultra-high performance concrete.

2.5.1 Normal Strength Concrete Models for Determining Prestress Losses

Many methods have been proposed to calculate prestress losses including lump sum, simplified methods, and incremental time-step methods. For most structural design applications the simplified approaches are appropriate. Due to the variability of prestress losses, even the most detailed approaches produce only an estimate and may over-estimate or underestimate the actual losses as shown by a probabilistic comparison (Gilbertson and Ahlborn 2004). To understand the methodology behind calculating prestress losses, it is important to consider all of the loss components that are associated with prestressing concrete. The first components of loss happen during the tensioning of strands in the prestressing facility before the concrete is placed. These components are due to friction, seating, and temperature effects. Generally these losses are the responsibility of the prestressing facility as they are dependent on the specific casting beds and prestressing equipment used by that facility. At the time of transfer, the precast element exhibits elastic shortening. This is a one-time loss but can contribute a significant amount of prestress loss at transfer. Once the prestressing strands are released or cut, the long-term loss components begin to act on the prestressed element. Long-term losses in pre-tensioned members include creep, shrinkage, and steel relaxation.

This research considered several techniques to determine that most applicable method for the calculation of prestress losses. The prestress losses are to be computed at the point of the span where the tensile forces of the prestressed element are most critical (PCI 2010). For this research all beams were analyzed at the mid-span.

2.5.1.1 Elastic Shortening

Three methods were considered when determining the elastic shortening component of the prestress losses. The first and most simplified of these methods was the gross-section approximation method, which is presented in the PCI Design Handbook (PCI 2010). This method, as seen in Equation 2.1, calculates the elastic shortening by multiplying the stress in the concrete at the level of prestressing strands (f_{cir}) by the modular ratio (E_{ps}/E_{ci}). The term K_{cir} represents a 10 % decrease in prestressing to account for the stress in the concrete after transfer and is taken at 0.9 for pretensioned members.

$$\Delta f_{pES} = \frac{E_{ps}}{E_{ci}} f_{cir} \quad [\text{Eqn. 2.1}]$$

Where

$$f_{cir} = K_{cir} \left(\frac{P_i}{A_g} + \frac{P_i e^2}{I_g} \right) - \frac{M_g e}{I_g} \quad [\text{Eqn. 2.2}]$$

E_{ps} = elastic modulus of prestressing steel

E_{ci} = elastic modulus of concrete

P_i = force in prestressing strands

e = distance from concrete centroid to strand centroid

I_g = gross moment of inertia

M_g = moment caused by dead load

The next method for calculating losses due to elastic shortening was similar to the gross section approximation method with the inclusion of an iterative process (ACI 423.X 2013).

The iterative gross section approach is more accurate because it accounts for the elastic shortening that happens immediately after the strands are cut. To account for this difference, a closed form solution is formulated by using the Equations 2.3 and 2.4 below and solving for Δf_{ps} to obtain equation 2.5 (Naaman 2010).

$$f_{pi} = f_{pj2} - \Delta f_{pR1} - \Delta f_{pES} \quad [\text{Eqn. 2.3}]$$

$$\Delta f_{pES} = n_{pi} \left[\frac{f_{pi}}{f_{pj2}} (f_{cgp})_{Fj} (f_{cgp})_G \right] \quad [\text{Eqn. 2.4}]$$

$$\Delta f_{pES} = \frac{(f_{cgp})_{Fj} [f_{pj2} - \Delta f_{pR}(t_0, t_t)] + (f_{cgp})_G f_{pj2}}{f_{pj2} / n_{pi} + (f_{cgp})_{Fj}} \quad [\text{Eqn. 2.5}]$$

Where

$$f_{pi} = f_{pj2} - \Delta f_{pR}(t_0, t_t)$$

$(f_{cgp})_{Fj}$ = stress in concrete at level of strands due to prestressing force

$(f_{cgp})_G$ = stress in concrete at level of strands due to dead load

$$n_{pi} = \text{modular ratio } (E_{ps} / E_c)$$

f_{pj2} = stress in strands after jacking losses, i.e. anchor loss and friction loss

$\Delta f_{pR}(t_0, t_t)$ = loss of strand stress due to relaxation from t_0 to t

The third and most accurate process reviewed for use in the calculation of elastic shortening was the transformed section approach (ACI 423.X 2013). This method makes three assumptions; linear elastic material behavior, perfect bond between concrete and steel reinforcement, and plane sections remain plane. The transformed section approach is more

accurate than the others because it accounts for the difference in modulus of elasticity between the concrete and the steel. The calculation of elastic shortening using the transformed section approach involves determining a new center of gravity and moment of inertia for the transformed section. Once the transformed section properties of the element are determined, the method of determining the elastic shortening is similar to above. Either the gross section approximation method or the iterative gross section method can be used with the transformed section properties. Differences in opinions exist as to whether the elastic shortening should even be considered when using the transformed section properties (AASHTO 2012). Current practice is that when using the transformed section properties to calculate prestressed losses, elastic shortening at time of release and elastic elongation due to externally applied loads during the service life of the element are subtracted from the total losses (AASHTO 2012).

2.5.1.2 Long Term Losses

Long-term prestress losses are those caused by the time dependent properties of concrete and steel. The calculation of long-term losses is a very complex calculation because each component of loss is continuously affected by the other components. To further complicate the calculation, these factors are dependent on uncertainties such as the time of loading, curing method, and environmental conditions (ACI 423.X 2013). Although they are not completely understood, there are many published methods for calculating long-term prestress losses.

The first method reviewed for the analysis of long-term prestress losses was the AASHTO LRFD refined method presented in the AASHTO LRFD Bridge Design Specification (AASHTO 2012). This method divides the long-term losses into two time periods: from release of prestress strands until the placement of the deck (with subscript id) and from placement of the deck until the end of the service life (df). The equation for prestress losses is as follows:

$$\Delta f_{pLT} = (\Delta f_{pSR} + \Delta f_{pCR} + \Delta f_{pR1})_{id} + (\Delta f_{pSD} + \Delta f_{pCD} + \Delta f_{pR2} + \Delta f_{pSS})_{df} \quad [\text{Eqn. 2.6}]$$

The AASHTO document presents equations for each of the components shown in the above equation (AASHTO 2012).

A second technique for computing long-term prestress loss was the age adjusted effective modulus approach, which was first introduced by Trost in 1967 (Wollmann et al. 2003). As described by Wollmann et al. (2003), the time dependent strain in the concrete is expressed as the sum of elastic and creep strains due to initial stress, elastic and creep strains due to change in stress, and the shrinkage strain. This relationship is expressed in Equation 2.7. The first term represents the elastic and creep strains due to an applied stress and the integral term represents the elastic and creep strains due to stress changes within the time interval between t and t_o .

$$\varepsilon_t = \frac{\sigma_0}{E_0} (1 + \varphi_{t,t_0}) + \int_{t_0}^t \left\{ \frac{1}{E(t)} \frac{d\sigma(t)}{dt} [1 + \varphi(1, t)] \right\} dt + \varepsilon_{st} \quad [\text{Eqn. 2.7}]$$

A simplified method, which was proposed by Trost, replaces the integral term by an aging coefficient, μ . The aging coefficient account for the reduced creep of concrete loaded at a

greater age, and is therefore a function of load history. An aging coefficient of one would imply that loading is done in a single step at time $t = t_0$. Upon developing the theory of age adjusted effective modulus, Bazant showed that when change in stress is included by creep and shrinkage, μ ranges from .5 to 1.0 and for concrete loaded between ages 10 and 100 days a value of 0.7 to 0.9 is appropriate (Bazant 1972).

The incremental time-step method is another method for predicting long-term losses. It is based on the theory of superposition of elastic and creep strains from increments of stress placed on a structure (ACI 423.X 2013). This repetitive computational procedure accounts for the interdependency of the steel relaxation, creep, and shrinkage. This procedure also allows for the designer to choose the time step that can account for a more accurate computation depending on the specific element's loading schedule. Typically, a small time step is used early in the service life and a larger time step is used at the prestressed element approaches the end of service. It should be noted that this technique is cumbersome and generally is computerized for increased efficiency. The detailed process for this method is described in Section 3.3 of this document.

2.5.2 Normal Strength Concrete Models for Determining Deflections

The calculation of prestress losses is critical to understanding the short and long-term deflections of concrete elements. Deflections not only lead to tensile cracking but can be obvious to the user and cause concern over the safety of the structure. Failure to control deformations in prestress elements can lead to reverse deflections that can cause roof drainage problems, uncomfortable ride conditions on bridges, and alignment and cracking

issues in buildings (Nawy 2010). ACI 318-11 limits deflections in buildings based on the location in the building and the likeliness to be damaged due to large deflections. The values for these limits range from $L/180$ to $L/480$ (ACI 318-11), where L is the span length.

2.5.2.1 Theoretical Derivation of Deflection Methods

The moment-area method is conveniently used in design for determining deflections because the moments along the length of the member are generally known at early stages of design. This method, which was first developed by Mohr, is based on the relationship between bending moment and curvature at any point on the flexural member (Naaman 2010). The deflection of a beam at any point is the area under the moment diagram from the reference point to the point in question.

Another method for determining deflections commonly used in practice is the method of virtual work. This approach relates a system of forces in equilibrium to a compatible system of displacements. The name of this method is derived from the virtual systems of forces or displacements that are introduced to the system. Generally for the calculation of beam deflection, only the effects of bending moments and shear are considered because the axial forces and twisting moments have little or no effect on the vertical deflections. Thus, the deflection of a beam, D_j , by method of virtual work at point j is given by

$$D_j = \int \frac{M_{uj}M}{EI} dl \quad [\text{Eqn. 2.8}]$$

Where M_{uj} is the moment caused by the virtual load, M is the moment caused by actual loads, and E and I describes the section properties of the beam (Ghali et al. 2009). Equation

2.8 shows the form for calculating deflection from virtual work caused by the bending moment. This form does not include deformations caused by shear or torsion.

Several other methods such as the conjugate beam method and the equivalent load method can also be used to calculate the deflections accurately.

2.5.2.2 Practical Determination of Short and Long-term Deflections

Short-term deflections should be calculated using one of the techniques described above taking into account the initial prestressing forces and the losses at that time period.

Design code, ACI (ACI 318-11), and design handbook, PCI (PCI 2010), present methods to calculating long-term deflections using factors along with the calculated initial deflections found through analysis methods.

ACI presents a method for calculating long-term deflections with the λ_{Δ} multiplier. The expression given below, Equation 2.9, details the calculation of this multiplier.

$$\lambda_{\Delta} = \frac{\xi}{1+50\rho'} \quad [\text{Eqn. 2.9}]$$

The term ξ is the time dependent factor and is determined from R9.5.2.5 in the ACI code and, ρ' is the reinforcement ratio of the compression steel in the concrete beam.

PCI Design Handbook (PCI 2010) also describes a method that uses multipliers on the initial deflections to calculate the long-term deflections. In this method, initial deflections are determined and multiplied by the values in table 5.8.2 of the PCI Design Handbook (PCI 2010) to calculate the long-term deflections.

Both of these methods are unsuitable for the estimation of deflection in UHPC beams because the relationships given in these methods were empirically determined from data obtained with normal strength concrete. The multipliers mainly represent concrete creep and shrinkage of NSC concrete which follows different relationships than UHPC.

A more detailed approach to determining long-term deflections is needed for UHPC elements. The incremental time step approach, described in section 2.5.2.1, accounts for the applied prestressing force at each stage and calculates a deflection at each stage. These deflections are additive and sum to the total long-term deflection at any age.

2.6 Deflection Data from UHPC bridges

With UHPC becoming more known in the United States, several bridges have been built with this new material. This research has paid particular interest to the work of the Iowa DOT and their designs of the bridge in Wapello County and the Jakway Bridge. As stated above in Section 2.3, these bridges are constructed with UHPC girders and were the first of their kind in the United States (Graybeal 2013). The prestress loss analysis in this paper uses both of these shapes in the prestress loss analysis for comparison between the measured results of these bridges and the results obtained from this research. The Iowa Highway Research Board has sponsored Iowa State University to complete extensive testing on these bridge girders and help aid in the design of the UHPC Bridge. The results of these tests are included below to provide a benchmark for this research (Wipf et al. 2009, Rouse 2011).

The first UHPC Bridge in the United States was constructed as a bridge replacement to span the Little Soap Creek in Wapello County, Iowa. The adequacy of the bridge design was verified through an experimental test program completed at Iowa State University (Wipf et al. 2009). This test program included material testing, large and small scale laboratory testing, and field testing.

The modified bulb tee used for Wapello County bridge girders is shown in Figure 2.1. Five strands are harped at two points and decline linearly along the web of the section. Seven wire, Grade 270, 0.6 inch strands run horizontally for the central 22 feet of the beam. An additional 24 0.6 inch strands are located in the bottom flange, 8 of which are debonded in the last 3.5 ft. of the beam and 16 which are debonded over the last 6.5 ft. Curing of these beams was very similar to a curing method used by Flietstra (Wipf et al. 2009). Once the concrete placement was finished, the beam underwent a steam cure at 140 °F for 12 hours. At this point it was determined the UHPC reached a strength of 12,000 psi and the strands were released. Following the prestressing strand release, the UHPC was heat treated at 194 °F for 48 hours.

design of this beam underwent laboratory and field testing to verify the adequacy of the design (Rouse 2011).

The shape used for the girders of this bridge was the innovative pi-shaped girder, which was first proposed by the FHWA and Graybeal (2009a). After testing the first generation pi shaped girder, concerns were revealed about the transverse deck stiffness, cracking behavior at service loads and the lateral live load distribution (Graybeal 2009a). This revelation led to the design of the 2nd generation pi-girder girder, which was modified to address those concerns. The cross section of the 2nd generation pi-girder used in Buchanan County is shown in Figure 2.3.

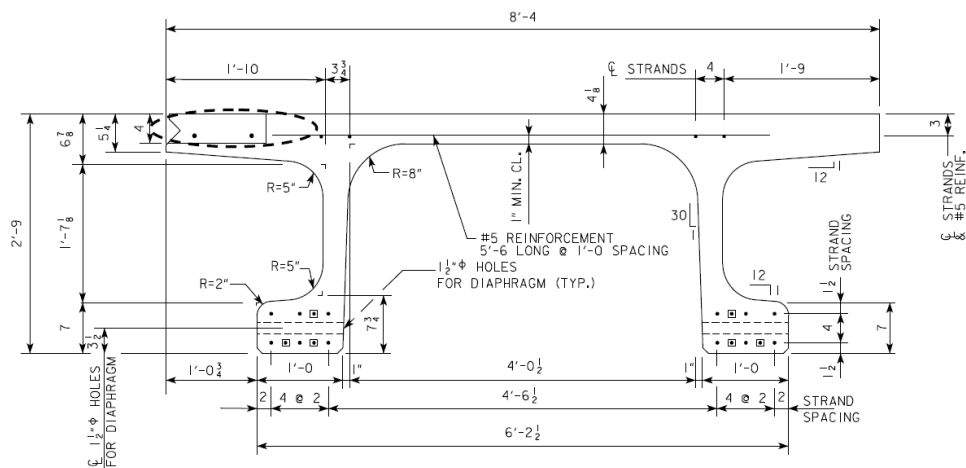


Figure 2.3 2nd Generation Pi-Girder (Rouse et al. 2011)

The beams were constructed in a similar fashion to those used for the bridge in Wapello County. After the concrete was placed, the forms were immediately covered and the girders underwent a thermal cure at 194 °F. The girders were removed from the forms after 25 hours and the strands were released at 40 hours. The release strength of the concrete was

12,500 psi. Laboratory testing for this beam consisted of compressive strength testing and flexural strength testing using specimens that were cast at the time of girder construction. Field testing of the Jakway Bridge involved monitoring strains and deflections of the bridge upon completion of the project and 1 year after completion. The tests used a known, tandem-axle dump truck crossing the bridge, and both static and dynamic testing was completed. No prestress loss calculations are presented in the report for the Jakway Bridge project.

2.7 Current UHPC Design codes

Publishing a design code is very important for the acceptance UHPC as a construction material. With national design codes, engineers will use the material more regularly in practice and have better confidence in the material performance. To date three design recommendations have been published on a national level dealing with UHPC. Australia, France, and Japan have led the way in this field (Gowripalan and Gilbert 2000, AFGC 2002, JSCE 2006) .

Australia released Design Guidelines for RPC Prestressed Concrete Beams in 2000 with the intent to provide guidelines for the design of prestressed beams using Ductal[®] (Gowripalan and Gilbert 2000). Where possible, the guidelines aimed to stay consistent with the limit states philosophy of the Australian Standard for Concrete Structures, AS3600-1994. Relying heavily on results published overseas, the authors used an approach based on the structural mechanics and material properties found in literature. Similar to design codes found in the

U.S., the Australian guides led to the design of prestressed RPC beams that are adequate in strength, serviceability, and durability.

The Australian guidelines characterize UHPC with regards to its behavior in compression, tension, modulus of elasticity, density, Poisson's ratio, creep, and shrinkage. It also provides design recommendations for strength in flexure, shear, and torsion, crack and deflection control, loss of prestress, and anchorage zones.

The prestressed losses section of this document outlines methods for short-term and long-term losses. The short-term loss recommendation is similar to that of gross section approximation method discussed in Section 2.5.1.1. The time-dependent loss recommendations call for a time step analysis of the cross-sections under consideration using the age-adjusted effective modulus method (Gowripalan and Gilbert 2000). This section also notes that techniques suggested by the Australian Standard for Concrete Structures (Gowripalan and Gilbert 2000) is an overestimate of losses and should not be used for UHPC.

In 2006, the Japan Society of Civil Engineers published Recommendations for Design and Construction of Ultra High Strength Fiber Reinforced Concrete Structure (Draft) (JSCE 2006). These recommendations prescribe a procedure for examining safety and serviceability performance metrics which are different from those of traditional reinforced concrete. The guidelines presented by the JSCE use the principles of design and construction to meet the performance requirements for safety, serviceability, durability, and resistance to fatigue.

Section 10 of the JSCE guidelines are written to address design of Prestressed UHPC members. The general guideline in this section is that all design topics be shall agree with the JSCE Standard Specifications for Concrete Structures – 2002 “Structural Performance Verification.”(JSCE 2006) With regards to prestress losses, the guidelines state that the loss of prestress due to shrinkage needs to be considered when designing with UHPC. It also states that a detailed study may be made to evaluate prestress timing, Young’s modulus, creep coefficient at early age, and effects of steel bars to determine the loss of prestressing force. The document provides no details regarding the calculation of prestress losses.

The AFGC-SETRA recommendations were composed by the French in 2002 and are composed of three parts (AFGC 2002). The first part provides specifications regarding the mechanical properties of UHPC, procedures to be used for placement, and construction inspections of finished products. The second part deals with design of UHPC structure and the third part deals with durability issues involved with UHPC. The design section, or Part 2 of the recommendations, builds off the French codes for prestress and reinforced concrete design but takes into account the strength introduced by the steel fibers. The recommendations give no guidelines regarding estimating prestress loss, but do state that heat treatment can significantly reduce creep, and that if nothing is known at preliminary stages regarding creep, the long-term creep coefficient can be taken as 0.8 without heat treatment and 0.2 with heat treatment (AFGC 2002).

Chapter 3 Analytical Plan

3.1 Modeling UHPC Time Dependent Properties

To account for the advanced material properties of UHPC, experimental test data was used to model certain parameters instead of using typical coefficients that have been proven to estimate the behavior of normal strength concrete. This section describes the data and techniques used to model UHPC creep, shrinkage and modulus of elasticity over time.

3.1.1 UHPC Creep Model

This research deals mainly with the effect of creep on prestress losses, so the importance of correctly describing creep for UHPC is paramount. The data used for the analysis in this work was obtained by Flietstra (2011) at Michigan Tech. Flietstra's data was chosen to model creep because of the curing regimes and loading regimes used mimic the prestressing industry norm. Through experimentation, Flietstra's data shows the creep strain of UHPC follows a curve until thermal treatment is applied. After thermal treatment, the creep strain follows a different model. Creep strain rapidly approaches a limit where it will exhibit very little to no additional creep once the thermal treatment is complete (i.e. properties are "locked-in"). It should be noted that although the creep coefficients obtained by Flietstra were different than previous UHPC compressive creep research, the predicted creep curve for ambient cured UHPC obtained from Flietstra's work predicts ultimate creep strains similar to previous work by Graybeal (Flietstra 2011). A function was fit to the data of ambient cured specimens. The form of this equation was chosen because it is standard in ACI when describing creep (ACI 209-92). This form was also chosen by Graybeal (2006) to

describe the compressive creep of UHPC. Equation 3.1 shows the relationship obtained by fitting the equation form to the data collected during testing by Flietstra (2011). A graphical representation of this equation is shown later in Section 3.3.2.

$$\varepsilon_{cr} = \frac{t^6}{4.069+t^6} * 1713 \quad [\text{Eqn. 3.1}]$$

Where ε_{cr} is the creep strain and t is the time in days after loading.

3.1.2 UHPC Shrinkage Modeling

The shrinkage of UHPC was also tested by Flietstra (2011). Equation 3.2 below was fit to shrinkage data that Flietstra (2011) obtained in conjunction with the creep results in order to determine basic creep. Equation 3.2 describes how the shrinkage strain was calculated for that component of prestress loss. A graphical representation of shrinkage strain for ambient conditions is shown later in Section 3.3.2.

$$\varepsilon_{sh} = 58.7 * \ln(t) + 122 \quad [\text{Eqn 3.2}]$$

Where ε_{sh} is the shrinkage strain at t days.

3.1.3 Modeling Elastic Modulus

Elastic modulus test data was used to develop a relationship to describe the change in modulus over time. To create this model, data was used from Peuse's work at Michigan Tech. (2006) Using elastic modulus data collected at 3, 7, 14, and 28 days, a curve was fit to represent the gain in elastic modulus for all ambient cured specimens. The relationship to compute the modulus of elasticity, at any time, E_{ci} , is:

$$E_{ci} = 418.09 * \ln(t) + 5281.5 \quad [\text{Eqn. 3.3}]$$

Where t is time from casting of the UHPC in hours.

To account for the fact the data for elastic modulus testing was recorded from the time of casting the cylinders, 72 hours was added to the time in the Matlab program. This is because the Matlab program sets the initial time ($t=0$) as the release of the prestressing strands, which were assumed to be cut 72 hours after the beam was cast.

3.2 Selection of Beam Shapes for Analysis

Three different sections were used during the prestress loss and deflection analysis to provide a broad range of applicability (see Table 3.1 for properties of each section). The first shape, a 12RB24 rectangular section (PCI 2010), was selected to provide a basic example of prestress loss and deflection calculation. The section was also used to verify the Matlab program against simple hand calculations (Appendix D). The author recognizes this shape does not optimize the advantages of UHPC. The results obtained from the analysis of the rectangular shape are not included in the results section of this thesis, but rather in Appendix B.

Table 3.1 Prestressed Concrete Beam Properties

	Section Type		
	Rectangular Section	Modified Bulb Tee	PI Shaped
Gross Section Area (in ²)	288	495.7	861
Gross Moment of Inertia (in ⁴)	13824	352516	105730
Linear Weight (kip/ft)	0.3	0.540	0.932
Distance from Neutral Axis to Bottom Fiber (in)	12	18.3	22.5
Span Length (ft)	50	110	87
# of prestressing strands at mid-span	10	47	18
Area of 0.6" ø Strands (in ²)	0.216	0.216	0.216
Distance from Strand Centroid to Bottom (in)	3.6	4.9	3.5

The second shape that was used in the research was the shape of the bridge girder used for the UHPC bridge designed by the Iowa DOT in Wapello County. The shape was a modified Iowa DOT Bulb Tee C standard. The dimensions of the cross section at mid-span are shown in Figure 3.1 (Wipf et al. 2009). For an analysis to be done on this shape assumptions were made on the concrete cover at the bottom of the section. The assumption was the strands at the bottom of the section were covered by 2 inches of UHPC. This dimension was chosen as it is typical of the strand spacing in the rest of the section and it meets the requirements for concrete cover on a bridge girder laid out by AASHTO LRFD Bridge Design Specifications (AASHTO 2012). The Wapello County bridge beams were 111 feet long and had a span of 110 feet, which was also the length used in the prestress loss and deflection analysis of this shape. The modified bulb tee is a reasonable approach to use UHPC with very common bridge shape. The Iowa Highway Research Board (Wipf et al.

2009) reports results from experimental and analytical testing to determine prestress losses and deflections of the modified bulb tee bridge.

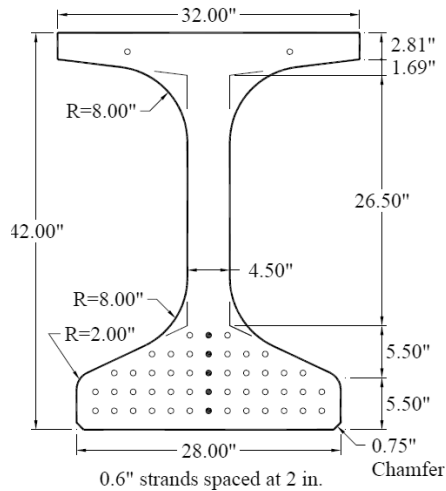


Figure 3.1 Cross Section of Modified Iowa Bulb Tee Girder (Wipf et al. 2009)

The third shape that was used in this analysis was the pi-girder used by the Iowa DOT for the Jakway Bridge, also in Iowa (Rouse et al. 2011). The shape was developed and optimized specifically to exploit the advanced mechanical and durability properties of UHPC (Graybeal 2009b). In-field testing was also completed on this bridge and is highlighted in the report by the Iowa Research Board (Rouse et al. 2011). The cross-sectional view of the pi-girder is shown in Figure 3.2.2.

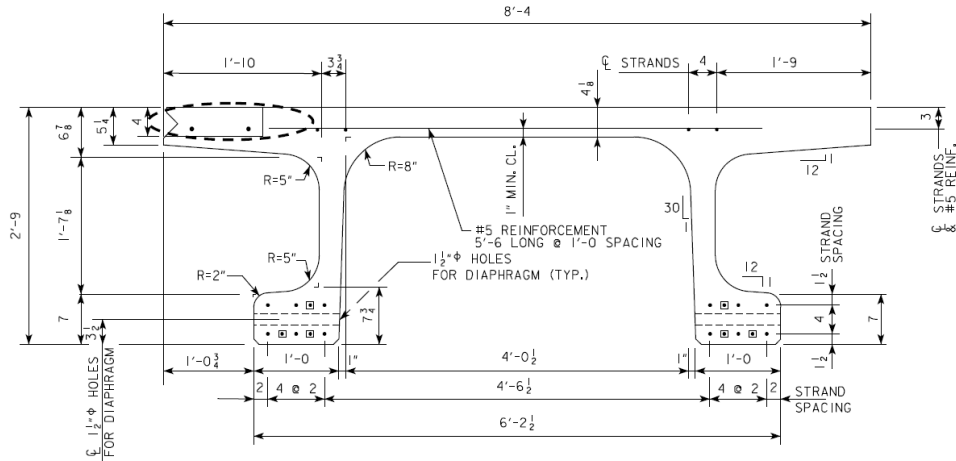


Figure 3.2 Cross Section of Pi-Girder (Rouse 2011)

The analysis also applied a deck on the modified bulb tee to simulate field conditions throughout the life of the structure. For the analysis to be complete, the composite section properties had to be determined. Figure 3.3 shows the shape of the composite section. The assumed deck thickness was 8 inches and the effective flange width was determined as 115 inches (AASHTO 2012). The centroid of the composite section is also dimensioned in Figure 3.3.

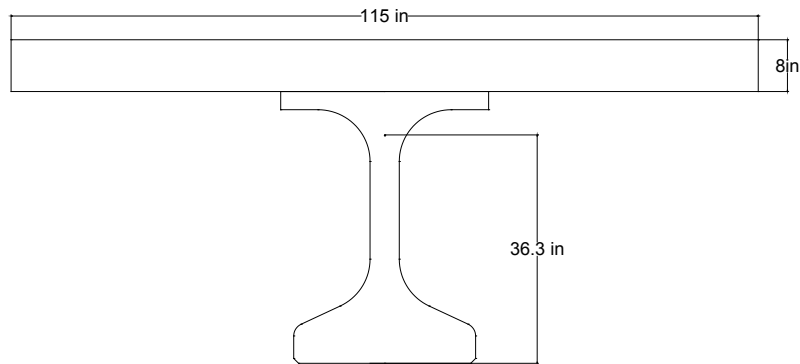


Figure 3.3 Cross Section of Composite Shape of Bulb Tee Section

3.3 Prestress Loss Calculation Methods

This section describes the methods used in the calculation of prestress losses for this research. Many approaches used to calculate prestress losses offer simplified methods for normal strength concrete using coefficients that are empirically derived. These approaches are not appropriate for this research as the behavior of the UHPC material is not yet well characterized. This section discusses the incremental time-step method programmed to calculate prestress losses accounting for variables such as thermal treatment and beam shape. The Matlab program is found in Appendix A.

Prestress losses are generally considered to start once the prestressing strands have been cut and the compressive forces transfer to the concrete element. For this research the instantaneous losses due to anchorage set and friction are not considered because they are generally accounted for by the prestressing facility. Losses due to anchor set and friction depend on the type of anchors and the methods for tensioning prestressing strands, both of which are dependent of the individual facility. To maintain similarity between the 3 different beams, 0.6 inch diameter low relaxations strands with an ultimate strength of 270 ksi were used in all three beams.

The first loss and only short-term component considered in this research was the prestress loss due to elastic shortening of the concrete member at the time of strand release. The closed form solution of the iterative method using the gross section properties was used to

compute the elastic shortening loss with one step as opposed to several iterations based on an initial guess. Equations 2.3 – 2.5 in Section 2.5.1.1 show the derivation of this solution.

After calculating prestress loss due to elastic shortening, the long-term losses were calculated using an incremental time step approach. This method is illustrated in multiple publications (Naaman 2010, Nawy 2010, ACI 423.X 2013). The first step of this procedure is to determine the creep strain and shrinkage strain during each time step. The models described in Section 3.1 are used in this step to determine the creep and shrinkage strains. The strain values are used to determine the amount of creep and shrinkage strain that occurred during that time increment. It should be noted that time steps should be chosen to include important loading stages in the life of the prestressed element and are generally smaller in the early phases and longer towards the end of the beams life.

Based on the general assumption of perfect bond between the concrete and the steel, prestress steel losses due to concrete creep and shrinkage were determined by summing the concrete creep and shrinkage strains, ϵ_{cr} and ϵ_{sh} , and multiplying that sum by the elastic modulus of the steel, E_{ps} . The step is shown in Equation 3.4.

$$\Delta f_{pCR+SH} = E_{ps}(\epsilon_{cr} + \epsilon_{sh}) \quad [\text{Eqn. 3.4}]$$

The stress lost due to steel relaxation of low-relaxation prestressing strands is calculated using Equation 3.5 between two time steps, t_i and $t_{(i-1)}$.

$$\Delta f_{pR} = f_{initial} \frac{\log(t_i - t_{(i-1)})}{45} \left[\frac{f_{initial}}{f_y} - .55 \right] \quad [\text{Eqn. 3.5}]$$

Where:

t = time in hours

f_{py} = yield stress of prestressing steel

$f_{initial}$ = strand stress at beginning of time step

The summation of the relaxation losses and the concrete creep and shrinkage losses determines the gross losses, $\Delta f_{p-gross}$, for that time step. With each time increment, the tendons will also experience an associated tendon stress increase. This occurs because the loss of prestressing force lessens the compressive stresses in the concrete at the level of the prestress. The reduction of concrete stress is in turn a strain in the concrete in the opposite direction of the prestressing force causing a small tensile increase in the prestressing strand, (i.e., causing the strand to “stretch”).

This increase in strand stress, or elastic rebound, is first based on the the change in concrete stress due to prestress loss. Using the basic principles of prestressed concrete to determine the change in concrete stress, $\Delta f_{conc.}$, at the centroid of the prestressing force, e , such that

$$\Delta f_{conc.} = \frac{P}{A_g} + \frac{P * e^2}{I_g} \quad [\text{Eqn. 3.6}]$$

Where

$$P = \Delta f_{p-gross} * A_{ps} \quad [\text{Eqn. 3.7}]$$

Where

$$\Delta f_{p-gross} = \Delta f_{pCR+SH} + \Delta f_{pR} \quad [\text{Eqn. 3.8}]$$

$$A_{ps} = \text{Total Area of Prestressing Steel}$$

The elastic rebound, a strand stress at the centroid of the prestressing force, is then computed by multiplying the concrete stress at the prestressing centroid by the modular ratio:

$$\Delta f_{pRebound} = \Delta f_{conc} * \frac{E_{ps}}{E_c} \quad [\text{Eqn. 3.9}]$$

Where

$$E_{ps} = \text{elastic modulus of prestressing steel}$$

$$E_c = \text{elastic modulus of concrete at the time step of interest}$$

After calculating the elastic rebound, the net loss and final strand stress can be determined for that time step by adding the stress gained from elastic rebound to the gross losses. This strand stress will be used as the initial prestressing force for the following time step.

3.3.1 Modeling for Ambient Curing Conditions of UHPC

The Matlab program was designed to analyze the prestress losses of the ambient cured beams before determining the losses for beams that were thermally cured. For ambient conditions, the functions that were derived for creep (Eqn. 3.1), and shrinkage (Eqn. 3.2), elastic modulus (Eqn. 3.3) were used to describe the behavior of the beam through the entirety of its life. Several conditional statements were used in the programing to ensure the stresses were evaluated correctly. For creep, shrinkage, elastic modulus, and steel relaxation, “if statements” were used to differentiate between the first step of the program and all of the following steps. This was important because within each time step, the losses that occurred

only during that increment were desired. To calculate the value of each loss component, the equations from Section 3.3 were used to determine the components' value for the end of the current time step, and then the value that was calculated at the end of the previous time step for that parameter was subtracted. An "if statement" was added that limited the steel relaxation equation to only subtract the prestress losses due to steel relaxation if the initial prestressing force for that time step was greater than 55 percent of the prestressing strand yield stress (Nawy 2010), else Eqn. 3.5 becomes negative and trivial.

3.3.2 Modeling for Thermal Treatment Curing Conditions

To determine the prestress losses of elements that underwent thermal treatment, as described by Flietstra, adjustments were made to the program written for the elements that were ambient cured. As described in Chapter 2, many studies have shown that when UHPC undergoes a thermal treatment, the creep and shrinkage are "locked in" and remain constant through the life of the element. With creep, once the element is finished with the thermal treatment, it has been found that $1650\ \mu\text{m}$ will be "locked in" with a load level of 60% of compressive strength (Flietstra 2011). Flietstra showed that creep was "locked in" and did not change with time for thermally treated UHPC specimens. It was also shown that creep strain will approach $1650\ \mu\text{m}$ no matter when the thermal treatment is applied. To account for this in the simulation of long-term prestress losses, a conditional statement was added to return a creep strain of $1650\ \mu\text{m}$ following the completion of thermal treatment. For each of the steps following the thermal treatment, the concrete experiences no additional creep strain. Figure 3.4 is a graphical representation of the creep strain models used for both ambient cured and the two thermal treatments scenarios.

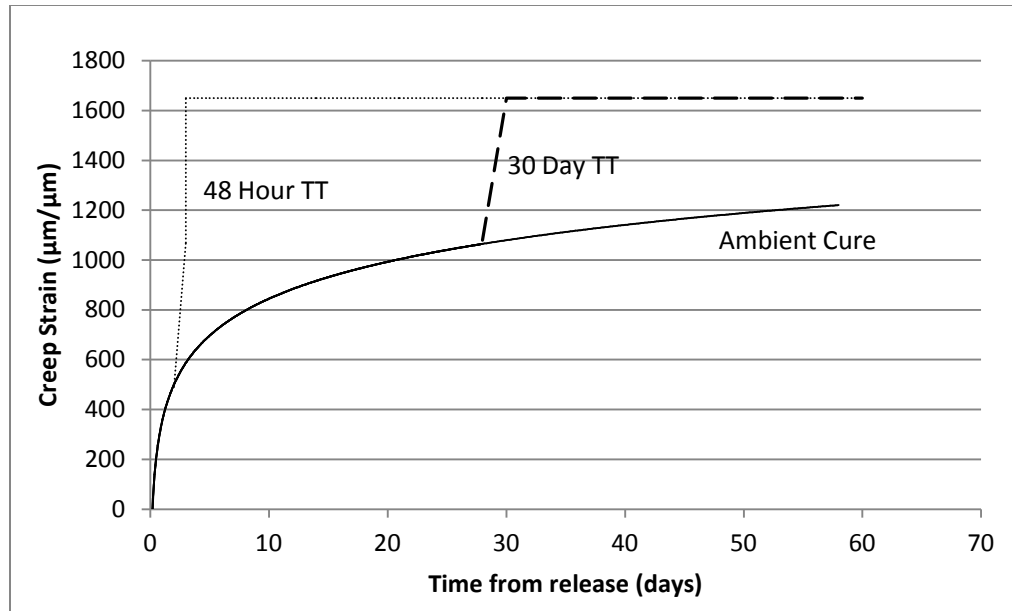


Figure 3.4 Creep Strain Models for Ambient Cured UHPC

The shrinkage strain was handled in a slightly different manner because experimental testing has shown that upon completion of the thermal treatment, the specimen will not exhibit additional shrinkage strain beyond the shrinkage strain the concrete has already endured (Flietstra 2011). To account for this, a conditional statement was added to the Matlab code that set shrinkage strain equal to 0 for all time steps past the determined time of the thermal treatment. Figure 3.5 graphically displays the shrinkage strain of UHPC over time for various curing regimes.

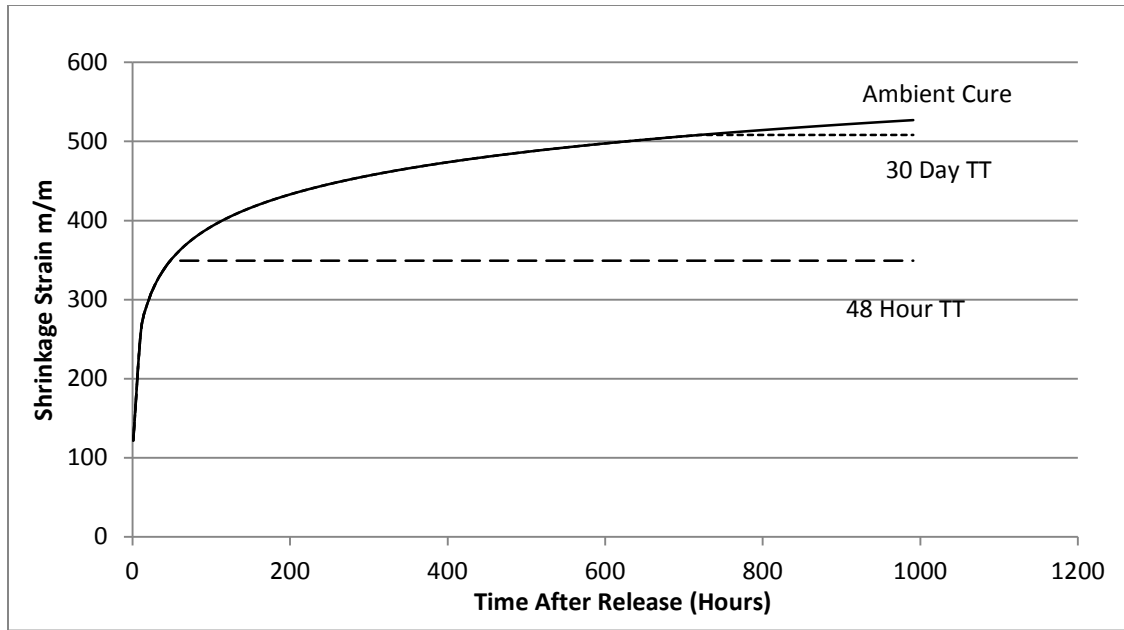


Figure 3.5 UHPC Shrinkage Strain Models used in Prestress Losses Analysis

Elastic modulus was also adjusted to account for pre-steam curing and thermal treatments because of the rapid change in stiffness that occurs in the matrix when the element undergoes these treatments. Testing reported by Ahlborn et al. (2011) shows that upon completion of thermal treatment the elastic modulus approaches 8130 ksi.

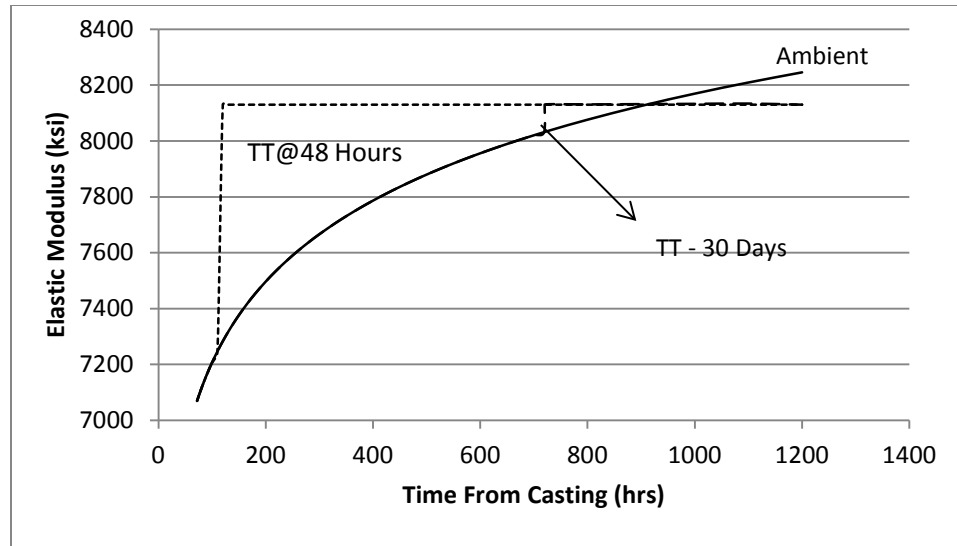


Figure 3.6 Modulus of Elasticity Models used in Prestress Losses Analysis

To ensure the programming was appropriately determining the creep strain, shrinkage strain, and elastic modulus hand calculations (Appendix D) were completed for several time steps and compared to the results of the program.

3.4 Short and Long-term Deflection

The final step in programming was determining the deflection that the beam would exhibit given the prestress losses it had incurred. Deflections were calculated at the end of each time step so that a clear estimate of the deflections could be had over the life of the structure. The deflections are divided into three terms: camber due to the prestressing effects, girder dead load deflection, and deck weight dead load deflection. The dead load deflection caused by the deck was applied after 60 days, which is the assumed time of deck construction. The deflection caused by dead weight, both girder and deck, follows traditional deflection analysis and is shown in Equation 3.10. Note that deflection is influenced by the changing elastic modulus; therefore thermal treatment will have an effect

on the deflection. After deck placement the stiffness is also affected by the increased moment of inertia from the composite section.

$$\Delta Dead Load = \frac{5wL^4}{384E_{ci}I} \quad [Eqn. 10]$$

Where

w = applied dead load

L = beam span

E = Modulus of elasticity at current time step

I = Moment of inertia

Prestressed concrete members are continuously subjected to sustained eccentric compressive loading due to the prestressing force. This force results in an upward deflection, called camber. Camber is used to counter downward deflections and is an important calculation because errors in camber can lead to unfavorable service conditions and beam sag. The equation that was used to calculate camber due to the prestress force is shown in Equation 3.11. This equation, similar to equation 3.10, is derived from the moment-curvature relationships.

$$Camber = -\frac{f_{ps}A_{ps}eL^2}{12E_{ci}I} - \frac{f_{ps}A_{ps}eL^2}{24E_{ci}I} \quad [Eqn. 3.11]$$

Similarly to dead load deflections, the elastic modulus and the moment of inertia are dependent on thermal treatment, time-step, and deck placement and, therefore, will effect deflection. After calculating the dead load and camber deflections individually the values were summed to account for the total deflection.

Chapter 4 Results and Discussion

This study consisted of applying an incremental time step prestress loss analysis for three different UHPC beam cases (rectangular section, modified bulb tee section, and pi-girder section) and three different thermal treatment regimens (ambient cure, 48 hour thermal treatment following casting, 30 day delay prior to thermal treatment) for each of those beam cases. The results from the modified bulb tee section and the pi-girder section are presented below. The time of $t=0$ was established as the point in which the prestressing strands were released. It should be noted that camber is taken as a negative deflection for the results presented herein. The purpose of the analysis of the rectangular section was to confirm the Matlab results with simple hand calculations (Appendix D); therefore the results are not presented as part of this section but rather can be found in Appendix B. The prestress loss and deflection results presented herein differ from previous studies because they considered the industry practice through modeling time dependent factors that affect prestress losses and subsequently deflection.

4.1 Bulb Tee Section Results

The modified bulb tee section results using ambient curing conditions are shown in Figure

4.1. These results are a graphical representation of the prestressing strand stress and the

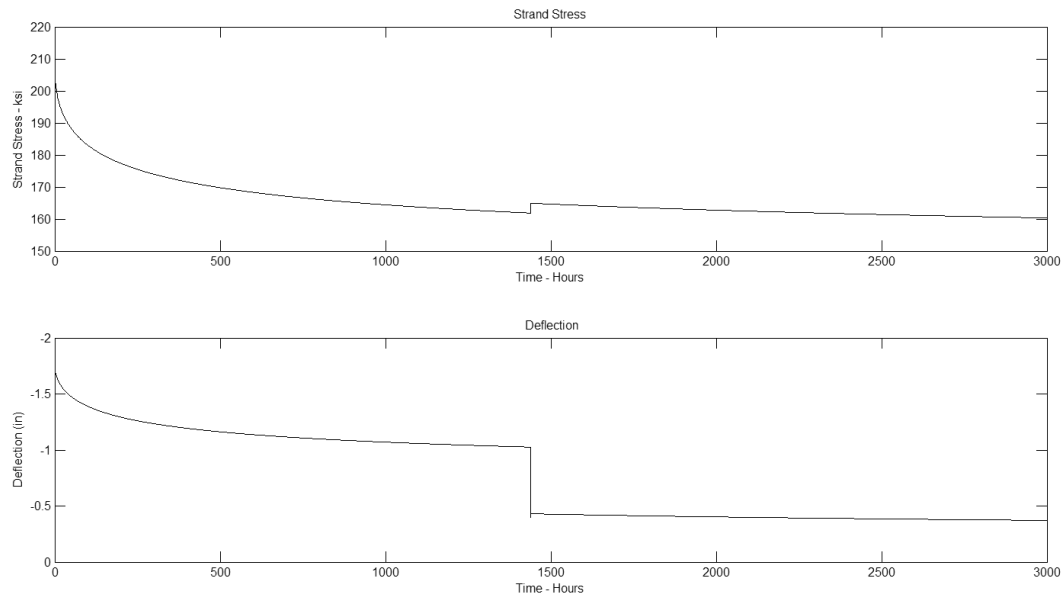


Figure 4.1 Prestress Loss and Deflection Results for Bulb Tee Section - Ambient Cure

deflection over time. The prestress losses are calculated for 10 years but are only shown in this figure for the first 3000 hours (125 days), which is true for Figures 4.2 and 4.3 as well.

The abrupt change, at 60 days (1440 hours), in strand stress and deflection is caused by the deck placement.

Figure 4.2 shows the estimated prestress losses and deflections for the modified bulb tee beam that was subjected to a thermal treatment 48 hours after the prestressing strands were released. This method is more typical of what might be expected in industry and is also recommend by UHPC suppliers. As before, the abrupt change at 1440 hours represents the

composite deck placement. In addition, the abrupt change at 48 hours represents the change in material behavior due to thermal treatment.

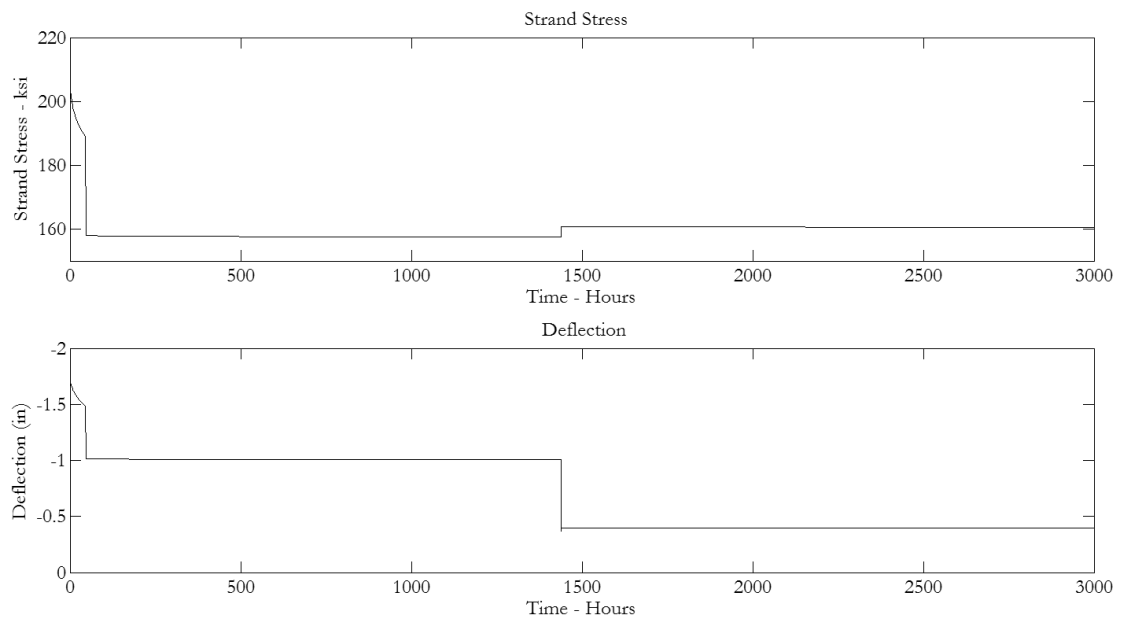


Figure 4.2 Strand Stress and Deflection for Modified Bulb Tee – Thermal Treatment at 48 Hours

Figure 4.3 shows the results of loss of prestress and deflections of a modified bulb tee that was subjected to thermal treatment 30 days after release of the prestressing strands.

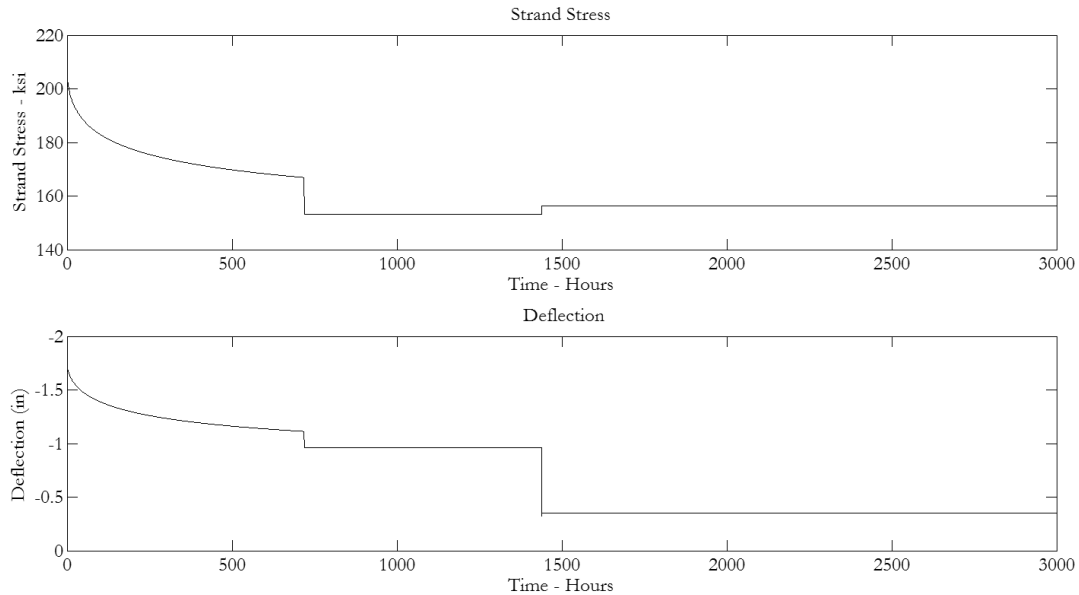


Figure 4.3 Strand Stress and Deflection for Modified Bulb Tee Thermally Treated at 30 Days

Similarly, the graph shows abrupt changes at 30 days (720 hours) due to thermal treatment and at 60 days (1440 hours) due to deck placement. Analysis was completed up to 10 years of service for the beam to determine the long term effects of the thermal treatment timing.

4.2 Pi-girder Results

The pi-girder was developed by FHWA as an attempt to optimize the mechanical properties of UHPC for bridges. The Jakway Bridge in Iowa was constructed using girders of this shape. The pi-girder beams were not subjected to deck placement in the analysis because the shaped does not require additional decking. The elastic gain and additional deflections caused by the cast-in-place UHPC joint connections that connect parallel girders were not

considered in this research. Figure 4.4 shows the prestress losses and deflections of the pi-girder subjected to ambient curing conditions.

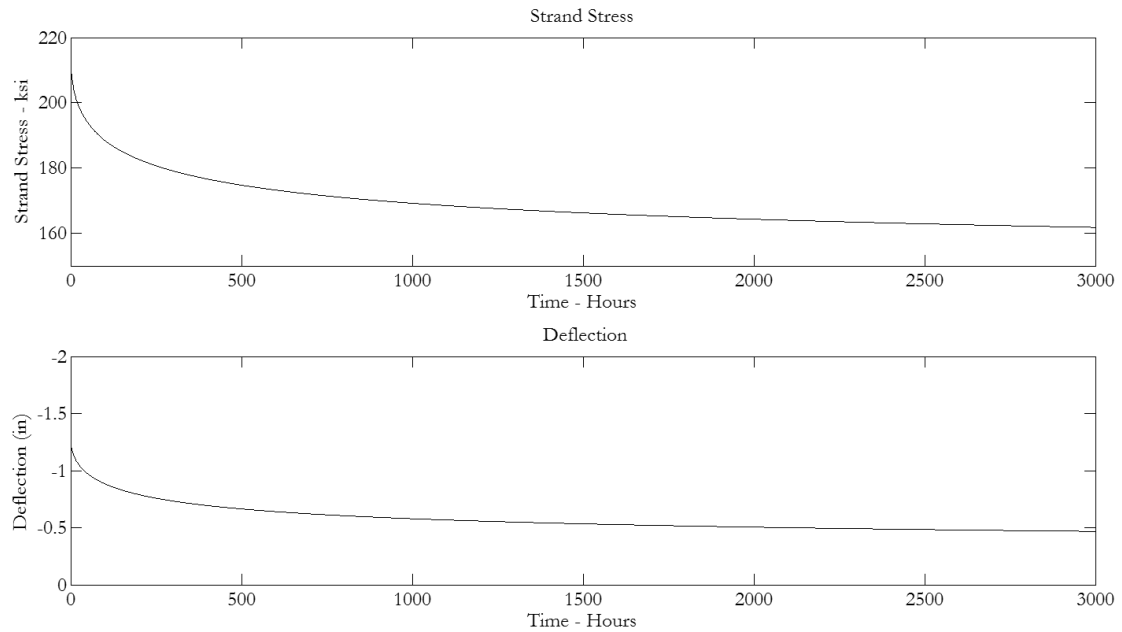


Figure 4.4 Strand Stress and Deflection for Pi-girder - Ambient Cure

Figure 4.5 shows the prestress losses and deflections of the pi-girder that was thermally treated 48 hours after release of prestressing strands. The figure below shows the results of the analysis for the first 3000 hours of service from when the prestressing strands are released.

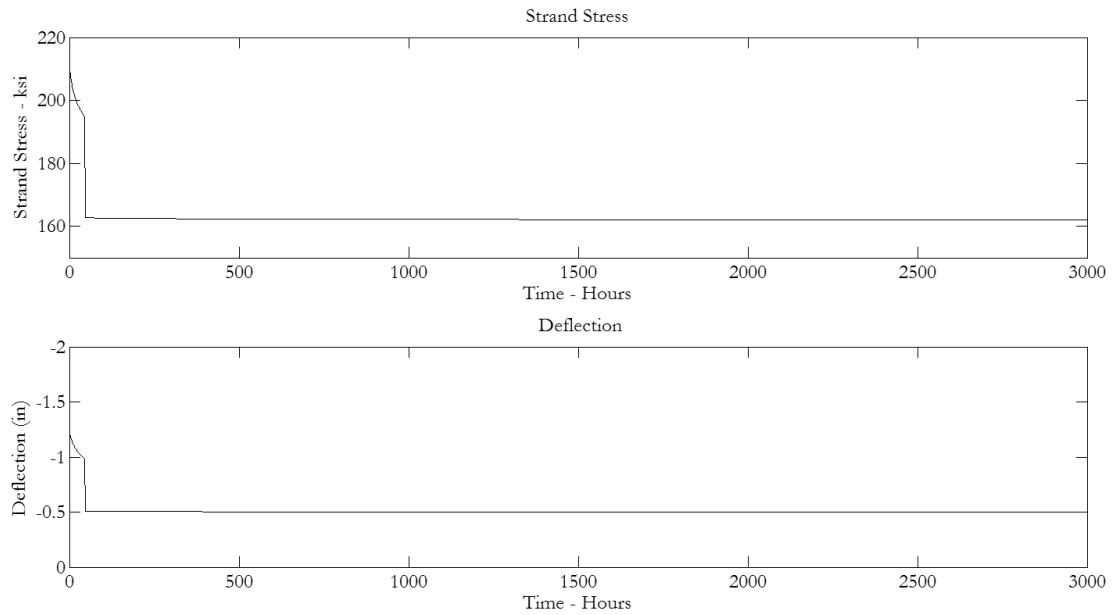


Figure 4.5 Strand Stress and Deflection for Pi-girder - Thermal Treatment at 48 Hours

Figure 4.6 shows the prestress losses and deflections of the pi-girder that was thermally treated 30 day after release of prestressing strands. The figure below shows the results of the analysis for the first 3000 hours of service from when the prestressing strands are released. Results for the first ten years of service for all shapes are discussed in Section 4.3.

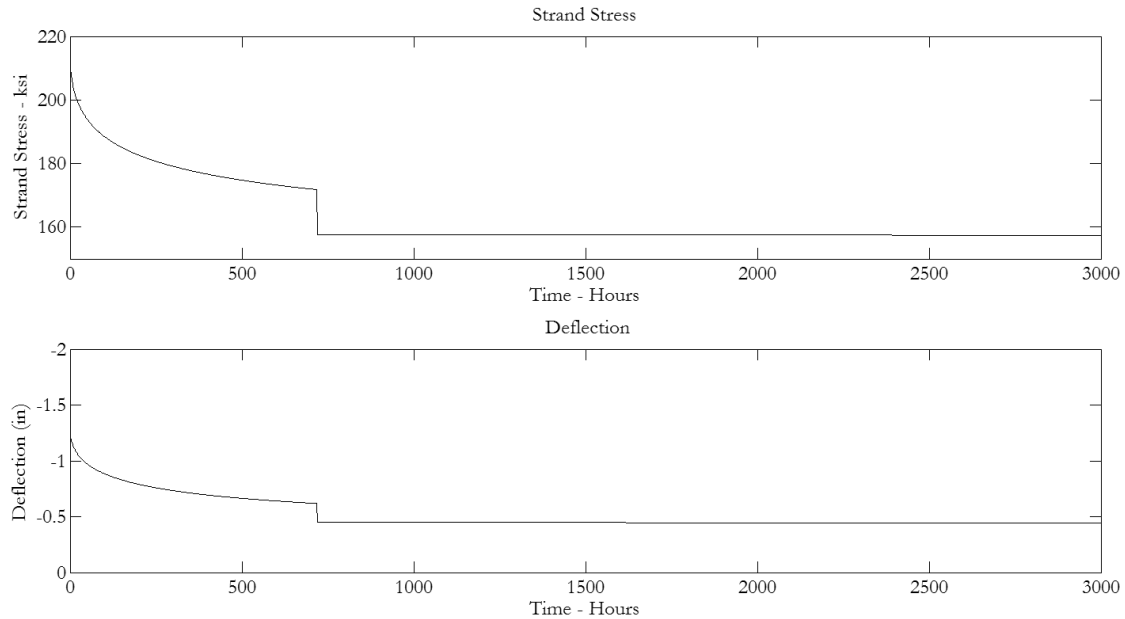


Figure 4.6 Strand Stress and Deflection for Pi-girder – Thermal Treatment at 30 Days

4.3 Discussion of Results

Four time steps are most critical during the life of the beam. For the discussion of the results presented in Sections 4.1 and 4.2, the values for strand stress, percentage of prestress loss, and deflections at the four critical time steps are compared. Critical times in the industry are at the time of release, construction, and long-term.

The first of the critical times is 100 hours after the release of prestressing strands. The time step was chosen because it is important to know the beams behavior after release. This time step also highlights differences in deflection due to thermal treatment 48 hour after release and thermal treatment that is delayed by 30 days.

The next critical time step highlighted is 60 days, before and after the placement of a cast-in-place deck. It is important for the engineer to understand the deflection of the beam if they are planning to use unshored construction at this stage of the beams life. This is especially

true of UHPC beams because the more slender the beam, the more its behavior is affected by flexural cracking. Controlling deflections before adding additional dead load will mitigate cracking at the bottom of section and improve the lifespan of the bridge. For the same reasons it is important to understand the behavior of the girders after the deck is placed. The final time step chosen for this research was 10 years after the beam was constructed. This time step gives a clear understanding of the long term effects of the timing of thermal treatment. It has been shown that beyond 10 years of service life, changes in prestress losses and deflections were negligible.

4.3.1 Strand Stress

4.3.1.1 Modified Bulb Tee

Table 4.1 shows the strand stress of the UHPC modified bulb tee section and the UHPC pi-girder section for the three curing regimes at each of the critical time steps. The strand stress shows how the thermal treatment affects prestress loss. In the modified bulb tee shape the strand stress for the beam that is subjected to thermal treatment 48 hours after release shows significant prestress losses during the first 100 hours. This is because after thermal treatment the compressive creep strain is locked to a value that is well above the creep strain for UHPC under ambient cure (see Figure 3.4). The results from the 48 hour thermal treatment simulation also show that after thermal treatment, UHPC exhibits minimal creep and shrinkage and, in turn, prestress loss. This finding was also observed by previous UHPC compressive creep research (Graybeal 2006).

Table 4.1 Strand Stress at Critical Time Steps

Shape	Curing Regime	Time After Release			
		100 Hours	60 days BD*	60 days AD*	10 years
Modified Bulb Tee	Ambient	183.0 ksi	161.8 ksi	164.9 ksi	147.8 ksi
	TT at 48 Hours	157.9 ksi	157.5 ksi	160.7 ksi	160.0 ksi
	30 Day Delayed TT	183.0 ksi	153.1 ksi	156.3 ksi	155.8 ksi
Pi-girder	Ambient	188.5 ksi	166.5 ksi		148.9 ksi
	TT at 48 Hours	162.6 ksi	162.1 ksi		161.5 ksi
	30 Day Delay TT	188.5 ksi	157.5 ksi		157.0 ksi

* BD denotes before placement of deck and AD denotes after deck placement

The prestress loss estimation results for the modified bulb tee that underwent a thermal treatment at 30 days after prestress release show differences in strand stresses beginning at 60 days. As shown at 100 hours in Table 4.1, the strand stress for the beam with the simulated 30 day delay in thermal treatment is the same as the strand stress for the beam that was cured in an ambient environment. This is because at 100, hours the prestress loss calculation is using the same models to compute creep strain, shrinkage strain, and elastic modulus.

At deck placement, the strand stress of the UHPC modified bulb tee beam that was thermally treated at 30 days after release shows little difference (4.4 ksi or 2% of the original jacking stress) compared to the beam that was subjected to thermal treatment 48 hours after release. This observation is important to understanding the importance of timing of thermal treatment.

Results from the 10 year time step (long term) show that if thermal treatment is delayed for 30 days as opposed to the thermal treatment shortly after release, the strands will experience as little as 5 ksi difference of prestress loss. Although the compressive creep strain,

shrinkage strain, and elastic modulus of UHPC are “locked-in” after thermal treatment, the timing of thermal treatment has only a small effect on the final prestress losses.

4.3.1.2 Pi-girder

The results for strand stresses at the critical time steps for the pi-girder are also given in Table 4.1. Many of the relationships that were observed for the modified bulb tee section were similar in the pi-girder section. The main difference between the sections was that the pi-girder girder was not stressed as highly as the bulb tee section. This beam, designed by the FHWA, only used 18 prestressing strands at the bottom of the section as opposed to the 47 strands that were used in the bulb tee section. One of the reasons for this was the pi-girder section was not designed to span as long of a distance. It should be noted that the pi-girder beam did not experience elastic gain due to deck placement because no deck was needed with this section.

Similar to the modified bulb tee section, the long term losses of the pi-girder girder show that a UHPC beam that is subjected to a thermal treatment shortly after release of prestress (48 hours) will experience less prestress loss than the same beam that is thermally treatment at 30 days after casting. However, the difference, 6.5 ksi or 2% of the initial prestress, is small.

4.3.2 Prestress Losses

Prestress loss is commonly presented or calculated in terms of the percentage of prestressing force that is lost after release of prestressing strands relative to the original jacking force. In

an article published by Post-Tensioning Institute, typical losses for a pretensioned beam are 19 percent of the initial jacking stress (ACI 423.X 2013). The PCI Design Handbook indicates that total prestress losses range from 12 to 25 percent for normally weight concrete and from 15 to 27 percent for lightweight concrete (PCI 2010). Table 4.2 shows the percentage of prestress loss for each of the critical time steps for the UHPC modified bulb tee section and the UHPC pi-girder section.

Table 4.2 Prestress Losses as Percentage of Initial Strand Stress

Shape	Curing Regime	Time After Release			
		100 Hours	60 days BD*	60 days AD*	10 years
Modified Bulb Tee	Ambient	19.9%	29.2%	27.8%	35.3%
	TT at 48 Hours	30.9%	31.0%	29.6%	30.0%
	30 Day Delay TT	19.9%	33.0%	31.6%	31.8%
Pi-girder	Ambient	17.5%	27.1%		34.8%
	TT at 48 Hours	28.8%	29.0%		29.3%
	30 Day Delay TT	17.5%	31.0%		31.3%

*** BD denotes before placement of deck and AD denotes after deck placement**

Table 4.2 shows that long term losses range from 30 percent of initial stress to 35.3 percent of initial stress for the modified bulb tee shape. Prestress loss analysis results are presented in the report of the modified bulb tee published by the Iowa DOT (Wipf et al. 2009). In this report, the prestress losses were calculated as 30.4 percent with assumed material behavior and 27 percent when calculated based on experimental results. These values compare well with the 30.0 percent loss of prestress calculated here for the modified bulb tee that was subjected to thermal treatment 48 hours after prestress release, which is representative of the actual curing sequence.

The pi-girder girder showed results that were very similar to the modified bulb tee in terms of percentage of prestress loss over the life of the beam. However, results show that early in the life of the structure the pi-girder girder losses less prestressing than the modified bulb tee. This is most likely because the stress in the concrete due to the prestressing force was less in the pi-girder girder.

4.3.3 Short and Long-Term Deflections

Prestress losses have no effect on the ultimate strength of a flexural component unless the effective prestress (or long term level of prestress) is less than 50 percent of the ultimate capacity of the prestressing strand. However, an over or under-estimation of prestress losses can have an impact on the serviceability limit states such as camber, deflection, or cracking (ACI 423.X 2013). Therefore, it is important to understand how the prestress losses affect the deflections of the beam over the service life. Table 4.3 shows the computed deflection results using prestress losses obtained from the incremental time-step method for the modified bulb tee section and the pi-girder section under various curing regimes.

Discussion answers three important questions regarding the relationship between prestress losses and deflections of UHPC beams. The effect of thermal treatment on deflection, deflections on ambient cured UHPC beam versus UHPC beams that are thermally treated, and the effect of thermal treatment timing on short and long term deflections are addressed in the following sections. Note that all deflections shown in Table 4.3 report a negative deflection. For this work downward deflection was considered the positive direction, therefore, a negative deflection represents an upward camber.

As previously discussed, several components of prestress loss are “locked-in” upon completion of thermal treatment. The effect of thermal treatment on prestress losses, in turn, has an effect on the deflection of the beam. Table 4.3 shows the computed deflections for both beam shapes at critical time-steps for all three curing regimes. As expected, ambient cured beams have the least camber remaining for long-term conditions. After thermal treatment, the UHPC beam experiences changes in deflection that are negligible (.05”) in the prestressed concrete industry.

Table 4.3 Deflections at Critical Time Steps

Shape	Curing Regime	<u>Time After Release</u>			
		100 Hours	60 days BD*	60 days AD*	10 years
Modified Bulb Tee	Ambient	-1.39 in	-1.03 in	-0.4 in	-0.21 in
	TT at 48 Hours	-1.01 in	-1.0 in	-0.4 in	-0.39 in
	30 Day Delay TT	-1.39 in	-0.96 in	-0.35 in	-0.34 in
Pi-girder	Ambient	-0.89 in	-0.54 in		-0.28 in
	TT at 48 Hours	-0.5 in	-0.5 in		-0.45 in
	30 Day Delay TT	-.89 in	-.45 in		-0.44 in

* BD denotes before placement of deck and AD denotes after deck placement

Note: Negative deflection represents and upward camber

The timing of thermal treatment may not affect the long term deflection of UHPC beams, but if the short term deflection is critical, the difference in deflection should not be ignored. The modified bulb tee that was subjected to thermal treatment 48 hours after prestress release shows nearly 0.38 in. more deflection than the beam in which thermal treatment was delayed 30 days. The computed deflection for the UHPC pi-girder at 100 hours showed similar results, with the timing of thermal treatment resulting in a .39 in. differential. This could be of importance to a prestressing facility that needs to know the deflections of beams for transportation purposes.

Chapter 5 Conclusions and Future Work

5.1 Conclusions

The purpose of this research was to determine if the timing of thermal treatment during the manufacturing procedure of two UHPC prestressed beams has an effect on long-term losses and deflections of UHPC beams. Prestress losses were estimated for three UHPC beams (rectangular section, bulb tee section, and pi-girder section) to understand the short and long-term deflections. The prestress losses were computed using an incremental time-step method and material models to account for differences due to the timing of thermal treatment if applied at all. This method allowed for losses to be computed at any desired time step. The time step method also allowed for computation of creep strains and shrinkage strains using models that were derived from data collected by Flietstra in which the manufacturing process was replicated (Flietstra 2011). All data to obtain the results of this research are based on test results from Lafarge's Ductal[®] UHPC, and contains 2% by volume steel fibers. The timing of thermal treatments used for the analysis presented herein, was chosen to represent upper and lower bound of feasible times for UHPC beams to be thermally treated after release of prestress.

These specific conclusions have been made based on the results reported using the prestress loss simulation:

- UHPC beams that are not thermally treated show increased prestressed losses and deflections. If a prestressing facility chooses not to thermally treat their UHPC beams, detailed estimations of long term deflections should be made.

- The timing of thermal treatment has negligible effects on long-term prestress loss or deflections for the UHPC beams studied.
- Past creep research has stated that creep and shrinkage are locked-in after UHPC has been thermally treated. This concept also applies to long-term prestress losses and deflections. After thermal treatment, the beams experience negligible prestress losses and deflections. Following thermal treatment, external loads such as deck placement or live load will be the only contributors to changes in prestress levels and deflection.

5.2 Future Work

The completion of this work has led to the author to understand areas of this topic that should be researched further. The industry needs more consistency in testing creep and other time dependent material properties for UHPC. This could be accomplished by developing standards similar to the ASTM testing standards that govern the testing of normal strength concrete. Also, the need for more compressive creep testing data of UHPC is important. Because this property is complex a larger data base would create a more consistent model for the material behavior.

A continuation of this research is to perform prestress loss analysis using the creep coefficients reported by previous researchers. A comparison the methods used in this research compared to values recommended by other research would be beneficial.

The final recommendation for future work is to complete full scale testing of long-term deflections on UHPC for validation of computational methods.

References

- AASHTO, (2012). *LRFD Bridge Design Specifications*, Sixth Edition, American Association of State Highway and Transportation Officials, Washington, DC.
- ACI Committee 209, (1992), (Reapproved 2008), *Prediction of Creep, Shrinkage and Temperature Effects in Concrete Structures (ACI 209R-92)*, American Concrete Institute, Farmington Hills, MI, 2011.
- ACI Committee 423, (2013 Draft), *Estimating Prestress Losses (ACI 423.X)*, American Concrete Institute, Farmington Hills, MI, 2011.
- Ahlborn, T.M., D.K. Harris, D.L. Misson and E.J. Peuse (2011). "Characterization of Strength and Durability of Ultra-High-Performance Concrete Under Variable Curing Conditions." Transportation Research Record: Journal of the Transportation Research Board **2251**(-1): 68-75.
- Ahlborn, T.M., E. J. Peuse, D.L. Misson. (2008). ULTRA-HIGH PERFORMANCE CONCRETE FOR MICHIGAN BRIDGES MATERIAL PERFORMANCE – PHASE I, MDOT Research Report RC-1525, Michigan Department of Transportation, Lansing, MI.
- AFGC, (2002), Association Française de Génie Civil , *Interim Recommendations for Ultra High Performance Fibre-Reinforced Concretes*.
- American Concrete Institute –ACI (2008), Building Code Requirements for Structural Concrete, Committee 318, ACI, Farmington Hills, MI,.

American Society for Testing and Materials International. (2013). "Annual Book of ASTM Standards".

ASTM C 39, Standard Test Method for Compressive Strength of Cylindrical Concrete Specimens. 2005.

ASTM C 512, Standard Test Method for Creep of Concrete in Compression. 2002.

Anon [Internet], "North American Ductal® Bridge Projects." Available at www.ductallafarge.com [Viewed November 21, 2013].

Bazant, Z.P., (1972) "Prediction of Concrete Creep Effects Using Age-Adjusted Effective Modulus Method." *ACI Journal*, V.69, No.4, April, pp. 212-217.

Bierwagen, D. and Abu-Hawash, A., (2005). "Ultra-High Performance Concrete Highway Bridge," *Proceedings of the 2005 Mid-Continent Transportation Research Symposium*, Ames, IA, August.

Bornstedt, G. and Shike, C., (2011) "Connecting Precast Prestressed Concrete Bridge Deck Panels with Ultra High Performance Concrete," *Proceedings of the PCI National Bridge Conference*, October 22–26, Salt Lake City, UT, Compact Disc, Paper 106.

Burkart, I. and Müller, H.S., (2008) "Creep and Shrinkage Characteristics of Ultra High Strength Concrete (UHPC)," *Proceedings of the Second International Symposium on Ultra High Performance Concrete*, Ed., Fehling, E., Schmidt, M., and Stürwald. S., Kassel University Press, Kassel, Germany, pp. 469–476.

Cheyrezy, M., Maret, V., and Frouin, L., (1995) "Microstructural Analysis of RPC (Reactive Powder Concrete)," *Cement and Concrete Research*, Vol. 25, No. 7, pp. 1,491–1,500.

- Dinges, T. (2009). The History of Prestressed Concrete: 1888 to 1963. Architictural Engineering and Construction Science. Manhattan, Kansas, Kansas State University. Master of Science.
- Flietstra, J.C. (2011). *Creep and Shrinkage Behavior of Ultra High Performance Concrete Under Compressive Loading With Varying Curing Regimes*. Houghton, MI: MS Thesis, Michigan Technological University.
- Francisco, P. F. Benboudjema., P. Rougeau, JM. Torrenti, (2012) “Creep and Shrinkage Prediction for a Heat-Treated Ultra High Performance Fibre-Reinforced Concrete,” *Proceedings of Hipermat 2012 3rd International Symposium on UHPC and Nanotechnology for High Performance Construction Materials*, Ed., Schmidt, M., Fehling, E., Glotzbach, C., Fröhlich, S., and Piotrowski, S., Kassel University Press, Kassel, Germany, 2012, pp. 325–331.
- Garas, V. Y., K. E. Kurtis, L.F. Kahn. (2012). "Creep of UHPC in tension and compression: Effect of thermal treatment." Cement & Concrete Composites **34**(4): 493-502.
- Ghali, A., Favre, R., and ElBadry, M. (2012). Concrete Structures – Stresses and Deformations: Analysis and Design for Serviceability, Spon Press, New York, NY.
- Gilbertson, C.G., and Ahlborn, T.M. (2004). “ A probalistic comparison of prestress loss methods in prestressed concrete beams”, PCI JOURNAL, V.49, No. 5, Sept-Oct, pp. 52-69.
- Gowripalan, N. and Gilbert, R.I., "Design Guidelines for Ductal Prestressed Concrete Beams," The University of New South Wales, Sydney, Australia, 2000

- Graybeal, B.(2006). “Material Property Characterization of Ultra-High Performance Concrete,” FHWA, U.S. Department of Transportation, Report No. FHWA-HRT-06-103, McLean, VA.
- Graybeal, B.A., (2009a) “Structural Behavior of a Prototype Ultra-High Performance Concrete Pi-Girder,” FHWA, U.S. Department of Transportation, Report No. FHWA-HRT-10-027.
- Graybeal, B.A., (2009b) “Structural Behavior of a 2nd Generation Ultra-High Performance Concrete Pi-Girder,” FHWA, U.S. Department of Transportation, Report No. FHWA-HRT-10-026, 114 pp.
- Graybeal, B.A., (2013) “Ultra-High Performance Concrete: A State-of-the-Art Report for the Bridge Community,” FHWA, U.S. Department of Transportation, Report No. FHWA-HRT-13-060.
- JSCE, (2006). *Recommendations for Design and Construction of Ultra High Strength Fiber Reinforced Concrete Structures (Draft)*, Japan Society of Civil Engineers, JSCE Guidelines for Concrete No. 9.
- Keierleber, B., Bierwagen, D., Wipf, T., (2008) and Abu-Hawash, A., “Design of Buchanan County, Iowa, Bridge, Using Ultra High-Performance Concrete and Pi Beam Cross Section,” *Proceedings of the 2008 PCI National Bridge Conference*, Precast/Prestressed Concrete Institute.
- Kollmorgen, G.A. (2004). *Impact of Age and Size on the Mechanical Behavior of an Ultra-High Performance Concrete*. Houghton, MI: MS Thesis, Michigan Technological University.
- Loukili, A., Richard, P., and Lamirault, J., (1998), “A Study on Delayed Deformations of an Ultra High Strength Cementitious Material,” *Fourth CANMET/ACI/JCI Conference*:

- Advances in Concrete Technology*, Publication No. SP-179, Ed., Malhotra, V.M.
American Concrete Institute, Farmington Hills, MI, pp. 929–950.
- Mehta, P.K., and Monteiro, P.J.M (2006). “Concrete Microstructure, Properties, and Materials.” The McGraw-Hill Companies, Inc., New York, NY.
- Moore, B., (2012). “Little Cedar Creek Bridge—Big Innovation,” *ASPIRE*, Spring, p. 27.

Available at <http://www.aspirebridge.org> [Cited April 20, 2012].
- Naaman, Antoine E., 2010, *Prestressed Concrete Analysis and Design*, Third Edition, Technopress

3000, Ann Arbor, MI.
- Nawy, E. G. (2010). Prestress Concrete : A Fundamental Approach. Upper Sadle River, NJ,

Prentice Hall.
- Neville, A. M. (1970). Creep of Concrete: Plain, Reinforced, and Prestressed. New York,

NY, American Elsevier Publishing Company, Inc.
- Nyland, E.M. (2009). *Early-Age Creep and Shrinkage Behavior of an Ultra-High Performance Concrete for Precast/Prestressed Concrete Applications*. Houghton, MI: MS Thesis, Michigan Technological University.
- Peuse, E.J. (2008), *Impact of Age at Thermal Treatment on the Mechanical Properties of an Ultra-High Performance Concrete*. Houghton, MI: MS Thesis, Michigan Technological University.
- Ozyildirim, C., (2011) “Evaluation of Ultra-High-Performance Fiber-Reinforced Concrete,”

Virginia Center for Transportation Innovation and Research, Report No.

FHWA/VCTIR 12-R1, Federal Highway Administration, McLean, VA.

PCI (2010), PCI Design Handbook, Seventh Edition, Chicago, Precast Concrete Institute.

Rouse, J. M., Wipf, T., Phares, B., Fanous, F., and Berg, O., (2011) *Design, Construction, and*

Field Testing of an Ultra High Performance Concrete Pi-Girder Bridge, Iowa Highway

Research Board (IHRB) Project TR-574, Iowa Department of Transportation.

Royce, M.C., (2011) "Concrete Bridges in New York State," *ASPIRE*, Fall, pp. 46–48.

Available at <http://www.aspirebridge.org> [Cited November 23, 2011].

Shutt, C.A., (2009) "UHPC Joint Provides New Solutions," *ASPIRE*, pp. 28–30.

Wille, K., Naaman, A.E., and Parra-Montesinos, G.J., (2011), "Ultra-High Performance

Concrete With Compressive Strength Exceeding 150 MPa (22 ksi): A Simpler Way,"

ACI Materials Journal, Vol. 108, No. 1, pp. 46–54.

Wipf, T., Phares, B., Sritharan, S., Degen, B., and Giesmann, M., (2009) *Design and Evaluation*

of a Single-Span Bridge Using Ultra-High Performance Concrete, Iowa Highway Research

Board (IHRB) Project TR-529, Iowa Department of Transportation.

Wollmann, G. P., R. B. Anderson, C.L. Roberts Wollmann, (2003). "Creep and Shrinkage

Effects in Spliced Prestressed Concrete Girder Bridges." PCI JOURNAL

(November - December): 92-105.

Appendix A - Prestress Losses Matlab Program

```
% Chris Mullen - 11/20/2013
% Timestep Prestress Losses for UHPC Beam

clc
fprintf('\t1 - Square\n\t2 - Bulb Tee\n\t3 - Pi Shaped\n>>');
Beam_Type = input('Beam Case:')

if Beam_Type == 1;
    b=12;
    h=24;
    A_g=288;
    I_g=13824;
    w_0=.3;
    c_bottom=12;
    L_ft=50
    number_strands=10;
    y_s=3.6;
    w_deck=.958;
    I_composite=74880;
    C_composite=24.18;
end
if Beam_Type == 2;
    A_g=495.7;
    I_g=352516;
    w_0=.540;
    c_bottom=18.3;
    L_ft=110;
    number_strands=47;
    y_s= 4.9;
    w_deck=.958;
    I_composite=604592;
    C_composite=36.3;
end
if Beam_Type ==3;
    A_g=861;
    I_g=105730;
    w_0=.932;
    c_bottom=22.5;
    L_ft=87;
    number_strands=18;
    y_s= 3.5;
    w_deck=0
    I_composite=I_g;
end

L=L_ft*12;
M_0=w_0*L_ft^2/8;
M_deck=(w_deck*L_ft^2)/8;
%*****Prestressing Steel Properties
```

```

% .6 Inch Diamter Strands
% 270 Psi Stength
%number_strands=10;

%Area of Individual Strand
A_strands=.216;
% Area of Prestressing Strand in beam
A_ps=number_strands*A_strands;
% Modulus of Steel
E_ps=28500;
%Ultimate Strength of Steel
f_u=270;
%Yield Strength of Steel
f_y=f_u*.9;
%Distance from strands to bottom of section
%y_s=3.6;
%Eccentricity of stands from centroid
e=c_bottom-y_s;
%*****Input the timing of thermal treatment
TT=input('How many hours after release is thermal treatment
applied? ')

%*****Determination of Time Step
figure;
%Assume element is loaded at 72 hours after casting
i = 0;
test_f_ps = zeros(1, length(1:1:87600));
test_td = zeros(1, length(1:1:87600));
for t = 2:1:87600;
    i = i + 1;
%*****Determination of Modulus of Elasticity over Time
% Modulus of Elasticity as function of time, t, in hours
if t < TT
    E_current=418.09*log(t+72)+5281.5;
else
    E_current=8130;
end
%***** Elastic Shortening at release

%Stress in steel before transfer
%jacking limit of .94 fy
f_jack = .94*f_y;

%Jacking Force
F_jack=f_jack*A_ps;

%Modular Ratio at Time step,n
n_p=E_ps/E_current;

% Elastic Shortening only acts oEGnnce at time of release
if t == 2;

% Loss of prestress due to elastic shortening

```

```

        Delta_f_pES = (A_ps*f_jack*(I_g+e^2*A_g)-e*M_0*A_g)...
                      / (A_ps*(I_g+e^2*A_g)+(A_g*I_g/n_p));

    else

        Delta_f_pES = 0;

    end

% Strand Stress after Elastic Shortening
    if t == 2
        f_initial=f_jack-Delta_f_pES;

    else
        f_initial=f_ps_current;

    end

% *****Long Term Losses

% *****Steel Relaxation for given time step
    if t== 2

        Delta_f_pRE=f_initial*((log10(t)/45)*(f_initial/f_y-.55));

    else if f_initial/f_y > .55

        Delta_f_pRE=f_initial*((log10(t)-log10(t-
1))/45)*(f_initial/f_y-.55));

    else
        Delta_f_pRE=0;
    end
end

% *****Losses Due to Creep and Shrinkage
% Determining Creep Strain at current time step
% Defining the Ambient Creep Curve
if t < TT

    if t == 2

        Creep_strain=((t)/24)^.6/(4.069+((t)/24)^.6))*1713;
    else

        Creep_strain=((t)/24)^.6/(4.069+((t)/24)^.6))*1713 -(((t-
1)/24)^.6/(4.069+((t-1)/24)^.6))* 1713;

    end

else
    if t == TT

```



```

        Creep_strain=1650-(((t-1)/24)^.6/(4.069+((t-1)/24)^.6))*1713;
    else

        Creep_strain=0;
    end
end
if t < TT

    if t == 2

        Shrinkage_strain=58.7*log((t)/24)+122;

    else

        Shrinkage_strain=(58.7*log((t)/24))+122-(58.7*log((t-1)/24)+122);

    end
else

    Shrinkage_strain=0;
end
if Shrinkage_strain < 0

    Shrinkage_strain=0;
else
    Shrinkage_strain=Shrinkage_strain;
end
%***** Loss of prestress due to creep and shrinkage
Delta_f_pCRSH=E_ps*((Creep_strain+Shrinkage_strain)/1000000);

%***** Gross Loss for time step

Delta_f_psGross=Delta_f_pCRSH+Delta_f_pRE;

%***** Determine change in concrete stress at strand level

Delta_f_c=Delta_f_psGross*(A_ps/A_g)+(Delta_f_psGross*A_ps*e^2/I_g);
%***** Determine the elastic rebound of steel

Delta_f_pRebound=Delta_f_c*(E_ps/E_current);

if t==1441

    Delta_f_EG=n_p*((M_deck*12)*(C_composite-y_s)/I_composite);

else

```

```

        Delta_f_EG=0;
    end

    %***** Net Losses for time step

        Delta_f_psNet=Delta_f_psGross-Delta_f_pRebound-Delta_f_EG;

    %***** Current Strand Stress

        f_ps_current=f_initial-Delta_f_psNet;
        test_f_ps(i) = f_ps_current;

    %***** Upward Deflection Based on Stand stress

        Camber= -
        (f_ps_current*A_ps*e*L^2/(12*E_current*I_g)+f_ps_current*A_ps*e*L^2/(24
        *E_current*I_g));

        DL_Deflection = 5*w_0/12*L^4/(384*E_current*I_g);

        if t>=60*24

Deck_Deflection=5*w_deck/12*L^4/(384*E_current*I_composite);
        else
            Deck_Deflection=0;
        end

        Total_deflection=Camber+DL_Deflection+Deck_Deflection;

        test_td(i) = Total_deflection;

    end

    tt = 1 : 1 : 87600;
        subplot(2,1,1)
        plot(tt,test_f_ps,'-k','LineWidth',.5)
        axis([0 87600 50 250])
        title('Ambient Cure Prestress Losses')
        xlabel('Time - Hours')
        ylabel('Strand Stress - ksi')

        subplot(2,1,2)
        plot(tt,test_td,'-k','LineWidth',.5)
        axis([0 87600 -3 2])
        title('Ambient Cure Deflections')
        xlabel('Time - Hours')
        ylabel('Deflection (in)')

```

Appendix B – Results of Rectangular Beam

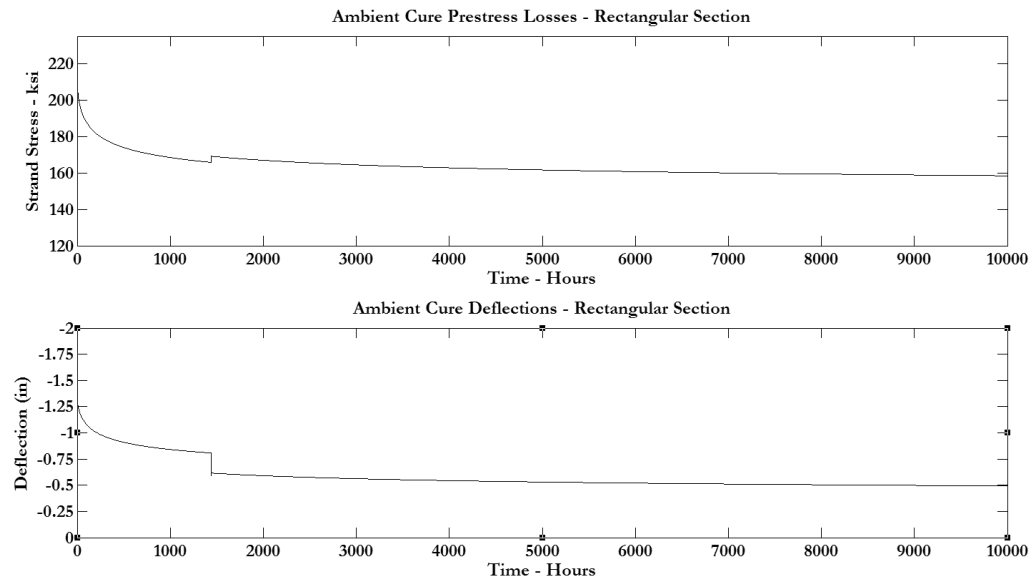


Figure B.1 Prestress Losses and Deflections for Ambient Cured Rectangular Section

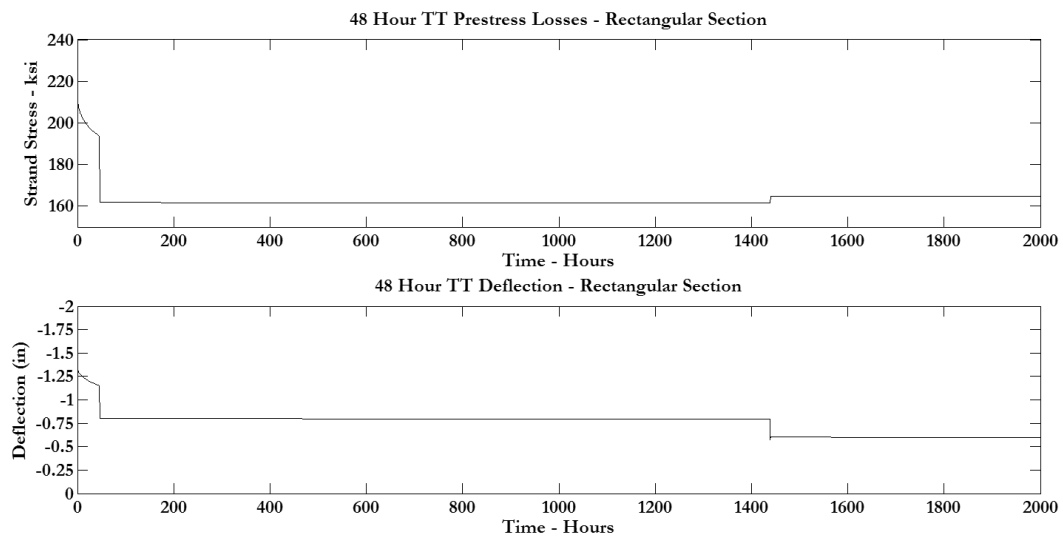


Figure B.2 Strand Stress and Deflections for Rectangular Beam Thermally Treated at 48 Hours

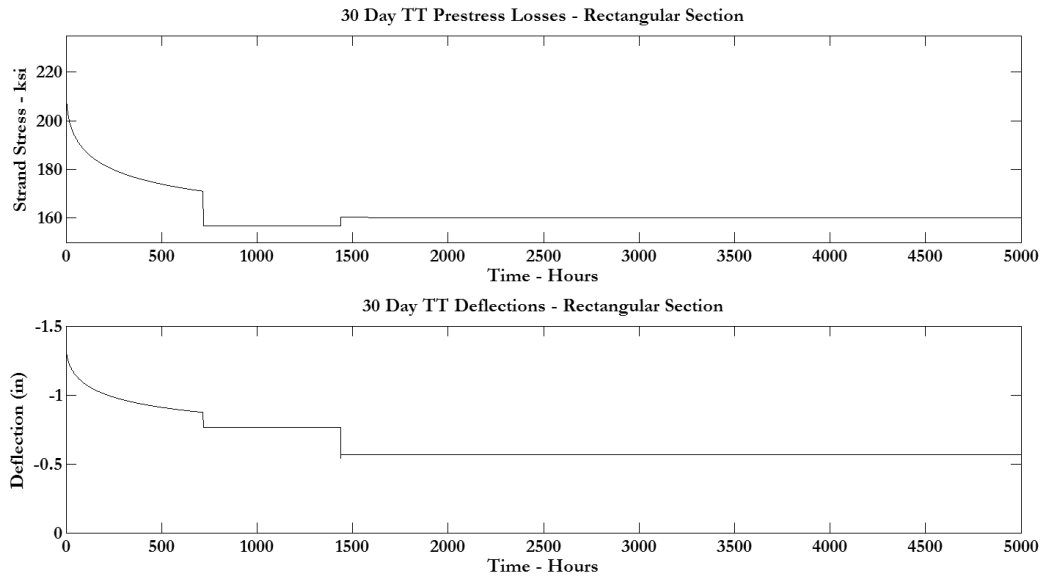


Figure B.3 Strand Stress and Deflections for Rectangular Beam Thermally Treated at 30 Days

Table B.1 Select Results for Strand Stress and Deflections of Ambient Cured Rectangular Section

Ambient Cure Results				
Time After Release	Prestress Strand Stress (ksi)		Deflection (inches)	
100 Hours	187.7		-1.08	
	<u>BD</u>	<u>AD</u>	<u>BD</u>	<u>AD</u>
60 Days	165.8	169.2	-0.808	-0.59
10 Years	151.5		-0.408	

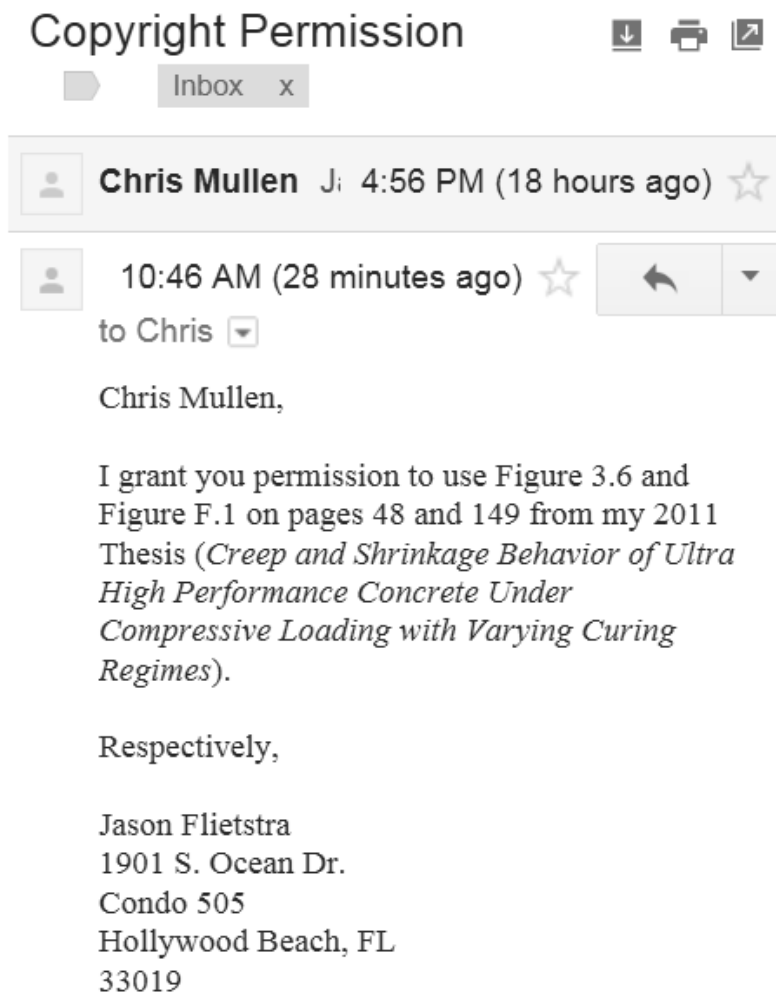
Table B.2 Select Results for Strand Stress and Deflections of Ambient Cured Rectangular Section

Thermal Treatment @ 48 Hour				
Time After Release	Prestress Strand Stress (ksi)		Deflection (inches)	
100 Hours	161.8		-0.803	
Deck Placement	<u>BD</u>	<u>AD</u>	<u>BD</u>	<u>AD</u>
60 Days	161.4	164.8	-0.797	-0.601
10 Years	164.1		-0.5953	

Table B.3 Select Results for Strand Stress and Deflections of Ambient Cured Rectangular Section

Thermal Treatment @ 30 Days				
Time After Release	Prestress Strand Stress (ksi)		Deflection (inches)	
100 Hours	187.7		-1.08	
Deck Placement	<u>BD</u>	<u>AD</u>	<u>BD</u>	<u>AD</u>
60 Days	156.8	160.3	-0.764	-0.568
10 Years	159.6		-0.563	

Appendix C – Copyright Permissions



Appendix D – Sample Calculations

Sample Calculation for Rectangular Beam - Ambient Conditions - 100 Hours After Release

$$t := 100$$

Section Properties [PCI Design Handbook 7th Ed. , 3-44]

Section - 12RB24

Section Dimensions:

$$b := 12 \cdot \text{in}$$

$$h := 24 \cdot \text{in}$$

Gross Section Area:

$$A_g := 288 \cdot \text{in}^2$$

$$w_0 := .3 \cdot \frac{\text{kip}}{\text{ft}}$$

Modulus of Elasticity at current time step:

$$E_{ci} := 418.09 \text{ksi} \cdot \ln(t + 72) + 5281.5 \text{ksi} = 7.434 \times 10^3 \cdot \text{ksi}$$

Gross Moment of Inertia:

$$I_g := 13824 \cdot \text{in}^4$$

Distance from N.A. to bottom face:

$$c_2 := 12 \cdot \text{in}$$

$$S_{xx} := 1152 \cdot \text{in}^3$$

Span:

$$L_{xx} := 50 \cdot 12 \cdot \text{in} = 600 \cdot \text{in}$$

$$r := \sqrt{\frac{I_g}{A_g}} = 6.928 \cdot \text{in}$$

$$y_s := 3.60 \text{in}$$

Eccentricity:

$$e_{xx} := c_2 - y_s = 8.4 \cdot \text{in}$$

Prestressing Properties

10 .6 inch diameter 270 stands

Area of Prestress:

$$A_{ps} := 10 \cdot .216 \text{in}^2 = 2.16 \cdot \text{in}^2$$

Ultimate Stress of Steel:

$$f_u := 270 \cdot \text{ksi}$$

Modulus of P/S steel:

$$E_{ps} := 28.5 \cdot 10^6 \cdot \text{psi}$$

Modular Ratio:

$$n := \frac{E_{ps}}{E_{ci}} = 3.834$$

$$f_{ci} := 14 \cdot \text{ksi}$$

Moment due to beam weight:

$$M_D := \frac{w_0 \cdot L^2}{8} = 93.75 \cdot \text{kip} \cdot \text{ft}$$

Yield stress of steel:

$$f_{py} := .9 \cdot f_u = 243 \cdot \text{ksi}$$

Jacking stress:

$$f_{jack} := .94 \cdot f_{py} = 228.42 \cdot \text{ksi}$$

Losses From Elastic Shortening

$$\Delta f_{pES} := \frac{A_{ps} \cdot f_{jack} \cdot \left(I_g + e^2 \cdot A_g \right) - e \cdot M_D \cdot A_g}{A_{ps} \cdot \left(I_g + e^2 \cdot A_g \right) + \frac{A_g \cdot I_g \cdot E_{ci}}{E_{ps}}} = 12.7 \cdot \text{ksi}$$

Initial Prestressing Force

$$f_{initial} := f_{jack} - \Delta f_{pES} = 215.72 \cdot \text{ksi}$$

Time Dependent Losses

Steel Relaxation

$$t_{\text{hours}} := 100$$

$$\Delta f_{pRE} := f_{initial} \cdot \frac{\log(100)}{45} \cdot \left(\frac{f_{initial}}{f_{py}} - .55 \right) = 3.238 \cdot \text{ksi}$$

Creep and Shrinkage Losses

$$t_{\text{days}} := \frac{t_{\text{hours}}}{24} = 4.167$$

Strain in Concrete due to creep:

$$\epsilon_{cr} := \frac{(t_{\text{days}})^{.6}}{4.069 + (t_{\text{days}})^{.6}} \cdot 1713 = 627.868$$

Concrete Strain due to shrinkage:

$$\epsilon_{sh} := 58.7 \cdot \log(t_{\text{days}}) + 122 = 158.382$$

Loss of P/S due to Creep and Shrinkage:

$$\Delta f_{pCRSH} := E_{ps} \cdot \frac{(\epsilon_{cr} + \epsilon_{sh})}{1000000} = 22.408 \cdot \text{ksi}$$

Gross P/S Losses:

$$\Delta f_{psGross} := \Delta f_{pCRSH} + \Delta f_{pRE} = 25.646 \cdot \text{ksi}$$

Change in Conc. Stress:

$$\Delta f_c := \Delta f_{psGross} \cdot \frac{A_{ps}}{A_g} + \frac{\Delta f_{psGross} \cdot A_{ps} \cdot e^2}{I_g} = 0.475 \cdot \text{ksi}$$

Gain in Prestress:

$$\Delta f_{\text{rebound}} := \Delta f_c \cdot n = 1.821 \cdot \text{ksi}$$

Change in Prestress due to Deck Placement

Weight of Deck: $w_{\text{deck}} := .958 \frac{\text{kip}}{\text{ft}}$

Moment Caused by Deck Weight: $M_{\text{deck}} := \frac{w_{\text{deck}} \cdot L^2}{8} = 299.375 \cdot \text{kip} \cdot \text{ft}$

Thickness of Slab: $H_{\text{slab}} := 8\text{in}$

Span := 50ft

Effective Flange Width : ACI 8.12.2

$$\text{EFW} := \min \left[.25 \cdot \text{Span}, 16 \cdot H_{\text{slab}} + 32\text{in}, \left(\frac{115\text{in} - 32\text{in}}{2} + \frac{115\text{in} - 32\text{in}}{2} \right) + 32\text{in} \right] = 115\text{in}$$

Area of Precast Section: $A_{\text{pc}} := 288\text{in}^2$

Area of Deck Section: $A_{\text{deck}} := 115\text{in} \cdot 8\text{in} = 920\text{in}^2$

Area of Composite Section: $A_{\text{composite}} := A_{\text{pc}} + A_{\text{deck}} = 1.208 \times 10^3 \cdot \text{in}^2$

Centroid of Composite Section: $C_{\text{composite}} := \frac{[12\text{in} \cdot A_{\text{pc}} + (24\text{in} + 4\text{in}) \cdot A_{\text{deck}}]}{A_{\text{composite}}} = 24.185\text{in}$

Moment of Inertia Precast: $I_{\text{pc}} := 13824\text{in}^4$

Composite Moment of Inertia:

$$I_{\text{composite}} := \left[I_{\text{pc}} + A_{\text{pc}} \cdot (C_{\text{composite}} - 12\text{in})^2 \right] \dots = 7.488 \times 10^4 \cdot \text{in}^4$$

$$+ \left[\frac{\text{EFW} \cdot H_{\text{slab}}^3}{12} + A_{\text{deck}} \cdot \left[\frac{H_{\text{slab}}}{2} + (24\text{in} - C_{\text{composite}}) \right]^2 \right]$$

Elastic Gain Due to Deck Placement: $\text{EG} := n \cdot \frac{(M_{\text{deck}}) \cdot (C_{\text{composite}} - y_s)}{I_{\text{composite}}} = 3.786\text{ksi}$

$$\Delta f_{\text{ps_net}} := \Delta f_{\text{psGross}} - \Delta f_{\text{rebound}} + \text{EG} = 27.611\text{ksi}$$

Current Steel Stress: $f_{\text{ps_100hours}} := f_{\text{initial}} - \Delta f_{\text{ps_net}} = 188.109\text{ksi}$

Deflections

$$\text{Camber} := - \left(\frac{f_{ps_100\text{hours}} \cdot A_{ps} \cdot e \cdot L^2}{12 \cdot E_{ci} \cdot I_g} + \frac{f_{ps_100\text{hours}} \cdot A_{ps} \cdot e \cdot L^2}{24 \cdot E_{ci} \cdot I_g} \right) = -1.495 \cdot \text{in}$$

$$\Delta_{dl} := \frac{5 \cdot w_0 \cdot L^4}{384 \cdot E_{ci} \cdot I_g} = 0.411 \cdot \text{in}$$

$$\Delta_{\text{deck}} := \frac{5 \cdot w_{\text{deck}} \cdot L^4}{384 \cdot E_{ci} \cdot I_{\text{composite}}} = 0.242 \cdot \text{in}$$

Deflections caused by deck to not act on girder until 60 days

Results from Sample Calculation:

$$\Delta_T := \text{Camber} + \Delta_{dl} = -1.084 \cdot \text{in}$$

From Results Obtained during Analysis:

Ambient Cure rectangular beam at 100 hours: $\Delta_{\text{total}} := -1.08 \text{ in}$